SLAC-158
UC-34
(EXPI)(ACC)

BEAM POLARIZATION EFFECTS IN HIGH ENERGY ELECTRON-POSITRON STORAGE RINGS

W. T. FORD and A. K. MANN

DEPARTMENT OF PHYSICS, UNIVERSITY OF PENNSYLVANIA*

Philadelphia, Pennsylvania 19104

and

T. Y. LING†

DEPARTMENT OF PHYSICS, UNIVERSITY OF WISCONSIN*

Madison, Wisconsin 53706

PREPARED FOR THE U. S. ATOMIC ENERGY

COMMISSION UNDER CONTRACT NO. AT(04-3)-515

November 1972

Printed in the United States of America. Available from National Technical Information Service, U. S. Department of Commerce, 5285 Port Royal Road, Springfield, Virginia 22151.
Price: Printed Copy $3.00; Microfiche $0.95.

---

*Research Supported in part by the U. S. Atomic Energy Commission.

†Present address: Dept. of Physics, University of Pennsylvania, Philadelphia, Pa.

ABSTRACT

Calculations are presented of beam polarization-dependent effects in high energy e^+e^- storage rings. The elastic scattering within a circulating bunch (Touschek scattering) leads to a net polarization-dependent effect of 5 to 10% for parameters appropriate to SPEAR, viz. $E_o = 2.5$ Gev, $\Delta E/E_o = 0.05$, and $\delta p_\perp = 0.6$ Mev, where E_o is the storage ring energy, ΔE is the average energy exchanged in the collisions and $\delta p_\perp$ is the width of the radial momentum distribution in the bunch. The final state angular distributions of the scattering processes $e^+e^- \to e^+e^-$, $e^+e^- \to \mu^+\mu^-$ and $e^+e^- \to \gamma\gamma$ are considerably modified by beam polarization, even for relatively low values of the time-averaged polarization. Calculations of counting rates and polarization-dependent effects for these e^+e^- collision processes are given.

TABLE OF CONTENTS

I. Introduction

It is expected[1] that the electron and positron beams in a storage ring become transversely polarized after their injection into the ring, with the positron polarization vector parallel to the guide field and the electron polarization vector antiparallel. The mechanism for this process is the interaction between the electron and the synchrotron radiation field, which results in unequal transition rates between the two states of spin orientation in the guide field. The effective temperature of the system is such that in the absence of depolarizing effects[11] the net polarization at equilibrium is[1]

$$P_o = \frac{8}{5\sqrt{3}} \simeq .924 \tag{1}$$

and the polarization P at any instant is

$$P(t) = P_o(1 - e^{-t/T}) \tag{2}$$

where the relaxation time T is given by[1]

$$T = \frac{8}{5\sqrt{3}} \frac{1}{\alpha} \left(\frac{mc^2}{\hbar c}\right) \frac{1}{c} \frac{1}{\gamma^5} R_{bend}^3 \times \frac{R_{ave}}{R_{bend}}$$

$$\simeq 98 \text{ sec} \times \frac{R_{bend}^3}{E^5(\text{Gev})} \times \frac{R_{ave}}{R_{bend}} \tag{2'}$$

In view of the potential usefulness of electron polarization as a tool in probing the structure of e^+e^- interactions[2], we have considered ways of detecting the polarization of the beams in SPEAR. For this machine equation (2') becomes

$$T \simeq \frac{165 \text{ hours}}{E^5 \text{ (GeV)}} \qquad (3)$$

or $T \simeq 1.7$ hour at 2.5 GeV. This is comparable to the anticipated lifetime of the beam, so appreciable polarization can be expected. Future higher energy (~ 4.5 GeV) beams at SPEAR would be approximately 92% polarized during most of the storage time.

II. Measurement of the polarization by means of the Touschek effect.

The relative motions of electrons within a bunch in the atorage ring are dominated by radial betatron oscillations; vertical betatron oscillations are present hut are generally much smaller. Longitudinal motions are also small, having momentum less than $\frac{\Delta E}{\gamma}$, where ΔE is the maximum deviation of the laboratory energy from the tuned value permitted by the RF and $\gamma = E_o/m_e$. The radial momenta are distributed over values which extend typically to about one electron mass depending on the storage ring energy and optical parameters (see Appendix). The exact form of the distribution is not of primary importance. A given pair of electrons can acquire appreciable longitudinal components of momentum from an elastic Møller scattering due to their relative motion within the bunch. In the laboratory these appear as deviations from the central energy greater than ΔE. This is an important mechanism which limits the beam lifetime in low

energy or high intensity storage rings; it has been calculated by several authors[1,3-5] and is often called the Touschek effect.

It is of particular interest that the Møller scattering cross section depends upon the polarization state of the electrons, which makes it possible, in principle at least, to detect the existence of beam polarization through this outscattering effect. The Touschek effect has been calculated in a nonrelativistic approximation by Bernardini, et al.[3], and relativistically by Gittelman and Ritson[4] who used a small-angle approximation to the Møller cross section. Völkel[5] used the exact Møller cross section for unpolarized electrons and a Gaussian distribution for the transverse momentum spectrum as well as the flat distribution of reference 4. Results of the corresponding calculation for polarized electrons have been presented by Baier[1]. In the remainder of this section we utilize these latter calculations to predict the magnitude of the net effect due to beam polarization to be expected in an outscattering or Touschek effect experiment at SPEAR.

The Møller cross section for transversely polarized electrons in their center of mass is[6,7]

$$\frac{d\sigma^*}{d\Omega}(\theta,\varphi) = \frac{r_o^2}{4p^{*4}E^{*2}} \frac{1}{\sin^4\theta} \left\{ 4 - 3\sin^2\theta + 4(4 - 3\sin^2\theta)p^{*2} + (4-\sin^2\theta)^2 p^{*4} \right.$$

$$- P_1P_2 \sin^2\theta \left[1 + 2(1 + \sin^2\varphi + \sin^2\theta \cos^2\varphi)\, p^{*2} \right.$$

$$\left. \left. + \sin^2\theta \cos(2\varphi) p^{*4} \right] \right\}, \qquad (4)$$

Here r_o is the classical electron radius, p^* and E^* are measured in electron masses, P_1 and P_2 are the magnitudes of the polarization vectors of the two electrons. The polarization axis is normal to the line of incidence of the

electrons and lies in the $\varphi = 0$ plane. The angles are defined in Fig. 1.

The Lorentz transformation to the laboratory is along the z-axis. The resultant laboratory angle of the scattered electron with respect to the z-axis (not indicated in Fig. 1) is very small, but the momentum change is significant and is intimately connected with the center-of-mass angle χ. Accordingly it is convenient to express the cross section in terms of the angles χ and ω, defined in Fig. 1, and integrate over the azimuth ω. From the figure,

$$\cos\chi = \sin\theta \sin\varphi \tag{5}$$

$$\sin\chi \sin\omega = \sin\theta \cos\varphi \tag{6}$$

The cross section in terms of χ and ω is

$$\frac{d^2\sigma^*}{d\cos\chi\, d\omega} = \frac{r_o^2}{4p^{*4}E^{*2}} \left\{ \frac{4}{(1 - \sin^2\chi\cos^2\omega)^2} - \frac{3 + P_1P_2}{1 - \sin^2\chi\cos^2\omega} \right.$$

$$+ \left[\frac{16 + 2P_1P_2\sin^2\chi\sin^2\omega}{(1 - \sin^2\chi\cos^2\omega)^2} - \frac{12 + 2P_1P_2(2 - \cos^2\chi)}{1 - \sin^2\chi\cos^2\omega} - 2P_1P_2 \right] p^{*2}$$

$$\left. + \left[\frac{16}{(1 - \sin^2\chi\cos^2\omega)^2} - \frac{8 + P_1P_2(\sin^2\chi\sin^2\omega - \cos^2\chi)}{1 - \sin^2\chi\cos^2\omega} + 1 \right] p^{*4} \right\} \tag{7}$$

The integration over ω yields after a lengthy computation

$$\frac{d\sigma^*}{d\cos\chi}(p^*, \cos\chi) = \frac{\pi r_o^2}{2p^{*4}E^{*2}} \left\{ \frac{2}{\cos^3\chi} - \frac{1}{\cos\chi} + 4\left(\frac{2}{\cos^3\chi} - \frac{1}{\cos\chi}\right)p^{*2} \right.$$

$$+ 2\left(\frac{8}{\cos^3\chi} + 1\right)p^{*4} - P_1P_2 \left[\frac{1}{\cos\chi} + \left(\frac{3}{\cos\chi} + 2 - \cos\chi\right)p^{*2} \right.$$

$$\left. \left. + (1 - 2\cos\chi)p^{*4} \right] \right\} . \tag{8}$$

In a storage ring the momentum p^* of the electrons viewed in the pair rest frame is distributed according to some function $F(p^*)$. Furthermore, the laboratory scattering angle is so small that the scattered electron almost always remains within the beam phase space. Only by its changed laboratory energy, E_1, is a scattered electron distinguishable experimentally from the other electrons in the beam. Accordingly we reexpress the cross section, equation (8), in terms of E_1 and p^*, and then integrate over the p^* spectrum to obtain the event rate as a function of E_1.

The connection between $\cos\chi$ and E_1 is

$$E_1 = \gamma(\beta p^* \cos\chi + E^*), \text{ where } \gamma = \frac{E_o}{E^*} ,$$

$$\text{i.e., } \cos\chi = (E_1 - E_o)\frac{E^*}{p_o p^*}$$

$$\simeq \frac{E^*}{p^*} \quad \frac{E_1 - E_o}{E_o} \quad .$$

Here E_o and P_o are the storage ring beam energy and momentum, respectively. It is particularly useful to define $\eta \equiv \frac{E_1 - E_o}{E_o}$, the fractional energy exchanged between the two electrons $\left[E_1 = E_o(1+\eta),\ E_2 = E_o(1-\eta)\right]$. In terms of η,

$$\cos\chi = \frac{E^*}{p^*}\eta \ . \tag{9}$$

With (9), equation (8) may be written

$$\frac{d\sigma^*}{d\eta} = \frac{\pi r_o^2}{2p^{*5}E^*}\left\{2\left(\frac{p^*}{E^*\eta}\right)^3 - \frac{p^*}{E^*\eta} + 4\left(2\left(\frac{p^*}{E^*\eta}\right)^3 - \frac{p^*}{E^*\eta}\right)p^{*2}\right.$$

$$+ \left(8\left(\frac{p^*}{E^*\eta}\right)^3 + 1\right)p^{*4} - P_1P_2\left[\frac{p^*}{E^*\eta} + \left(3\frac{p^*}{E^*\eta} + 2 - \frac{E^*\eta}{p^*}\right)p^{*2}\right.$$

$$\left.\left. + \left(1 - 2\frac{E^*\eta}{p^*}\right)p^{*4}\right]\right\} . \tag{10}$$

To get the event rate we compute the product (no. of targets) x (flux) x (cross section). It is convenient to use the laboratory frame of reference, in which all electrons have to a good approximation the same energy, E_o. Consider two electrons whose trajectories make the (small) angles θ_1 and θ_2 with respect to the nominal beam direction. The normal components of momentum are $p_{1\perp} = p_o\theta_1$ and $p_{2\perp} = p_o\theta_2$. The momentum p* of each electron with respect to the pair rest frame is

$$p^* = \tfrac{1}{2}\,(p_{2\perp} - p_{1\perp}). \tag{11}$$

The number of target electrons in an element of volume dV having radial momenta between $p_{1\perp}$ and $p_{1\perp} + dp_{1\perp}$ is $\rho dV\, f(p_{1\perp})dp_{1\perp}$, where ρ is the electron density and $f(p_{1\perp})$ is the normalized distribution of radial momenta. The flux of electrons in $dp_{2\perp}$ at $p_{2\perp}$ is $\rho v\ f(p_{2\perp})dp_{2\perp}$, where v is the relative velocity of the two electrons, given by $v = 2\frac{p^*}{E_o}c$. The cross section, being an area oriented parallel to the beam, is contracted by the factor $\frac{1}{\gamma} = \frac{E^*}{E_o}$ when transformed to the laboratory:

$$\frac{d\sigma}{d\eta} = \frac{E^*}{E_o}\,\frac{d\sigma^*}{d\eta}\ . \tag{12}$$

Collecting all these factors we write for the interaction rate

$$d^3\left[\frac{d^2W}{dtd\eta}(p^*,\eta)\right]dp^* = \rho dV f(p_{1\perp})p(2\frac{p^*}{E_o}c)f(p_{2\perp})dp_{2\perp}\,\frac{E^*}{E_o}\,\frac{d\sigma^*}{d\eta}\ ,$$

with the condition (11) relating p*, $p_{1\perp}$ and $p_{2\perp}$. This constraint can be inserted explicitly by means of a δ - function:

$$d^3\left[\frac{d^2W}{dtd\eta}(p^*,\eta)\right] dp^* = \frac{2c}{E_o^2}\,\rho^2 dV p^* E^* \frac{d\sigma^*}{d\eta}\, f(p_{1\perp})\, f(p_{2\perp})$$

$$\times\, \delta(\tfrac{1}{2}(p_{2\perp}-p_{1\perp})-p^*)\,dp_{1\perp}dp_{2\perp}dp^* \qquad (13)$$

To avoid double-counting the electron pairs we restrict the integration over transverse momenta to $p_{2\perp} > p_{1\perp}$:

$$\int_{-\infty}^{\infty} dp_{2\perp} \int_{-\infty}^{p_{2\perp}} dp_{1\perp}\; f(p_{2\perp})\, f(p_{1\perp})\delta(\tfrac{1}{2}(p_{2\perp}-p_{1\perp}) - p^*)$$

$$= \tfrac{1}{2}\int_{-\infty}^{\infty} dp_{2\perp} \int_{-\infty}^{\infty} dp_{1\perp}\, f(p_{2\perp})\, f(p_{1\perp})\delta(\tfrac{1}{2}(p_{2\perp}-p_{1\perp})-p^*)$$

$$= \int_{-\infty}^{\infty} dp_{2\perp}\, f(p_{2\perp})\, f(p_{2\perp} - 2p^*)$$

$$\equiv \tfrac{1}{2}F(p^*) \qquad (14)$$

where the first step follows from the symmetry of the integral under $p_{1\perp} \leftrightarrow p_{2\perp}$, and a factor of 2 has been included in the definition of $F(p^*)$ in order to have $\int_{-\infty}^{\infty} F(p^*)dp^* = 1$. The volume of the beam is defined by

$$\frac{N^2}{V} = \int \rho^2 dV\ , \qquad (15)$$

where N is the total number of electrons in a bunch. With (14) and (15) the interaction rate, (13) becomes

$$\frac{d^2W}{dtd\eta}(p^*,\eta) = \frac{N^2 c}{VE_o^2}\, p^* E^* \frac{d\sigma^*}{d\eta}\, F(p^*) \qquad (16)$$

The factor $p^*E^*\, d\sigma^*/d\eta$ is plotted in Fig. 2 as a function of p^* with η as a parameter taking on the values $\eta = 0.03$, 0.1, and 0.3; this is done for both complete polarization and no polarization. The threshold value of p^* for the process is given by equation (9) with $\cos\chi = 1$: $p_t^* = E_t^*\eta$; $p_t^* = \eta m_e/\sqrt{1-\eta^2}$. At threshold the rate for fully polarized electrons vanishes. This is a consequence of the antisymmetry requirement for the

wave function of a pair of identical fermions. Note that cos $\chi = 1$ corresponds to a scattering angle $\theta = 90$ degrees. This is a symmetric configuration, and the spin state is also symmetric, hence the overall final-state wave function vanishes.

The total count rate receives contributions from scatterings with all values of p^* present in the bunch. Fig. 2 shows that the events occurring just above threshold are sensitive to the polarization. The higher p^* scatterings serve to dilute the net effect.

If the distribution $f(p_\perp)$ of the radial momenta is Gaussian, then $F(p^*)$ is also Gaussian, with a width smaller by $\frac{1}{\sqrt{2}}$:

$$f(p_\perp) = \frac{1}{\sqrt{2\pi}\,\delta p_\perp} e^{-\frac{1}{2}\frac{p_\perp^2}{(\delta p_\perp)^2}} \quad , \tag{17}$$

$$\begin{aligned} F(p^*) &= \frac{2}{2\pi(\delta p_\perp)^2} \int_{-\infty}^{\infty} dp_\perp \, e^{-\frac{1}{2}\frac{p_\perp^2 + (p_\perp - 2p^*)^2}{(\delta p_\perp)^2}} \\ &= \frac{2}{2\pi(\delta p_\perp)^2} \, e^{-\frac{p^{*2}}{\delta p_\perp^2}} \int_{-\infty}^{\infty} dp_\perp e^{-\frac{(p_\perp - p^*)^2}{(\delta p_\perp)^2}} \\ &= \frac{1}{\sqrt{2\pi}\,\delta p^*} \, e^{-\frac{1}{2}\frac{p^{*2}}{(\delta p^*)^2}} \quad , \end{aligned} \tag{18}$$

where

$$\delta p^* = \delta p_\perp / \sqrt{2} \tag{19}$$

In SPEAR at 2.5 GeV the electrons have $\delta p_\perp$ between 0.4 and 0.9 MeV, hence δp^* between 0.3 and 0.6 MeV. We can estimate from Fig. 2 that with, say, $\eta = 0.1$ the net effect in the scattering due to polarization will be between 5 and 10 percent. The net effect increases at larger values of η, but the counting rate falls very rapidly as η increases.

Taking into account the threshold condition on p^*, the integral of equation (16) with respect to p^* becomes

$$\frac{d^2W}{dtd\eta}(\eta) = \frac{N^2c}{VE_o^2} 2\int_{\eta/\sqrt{1-\eta^2}}^{\infty} p^*E^* \frac{d\sigma^*}{d\eta} F(p^*)dp^* , \tag{20}$$

$$\equiv \frac{N^2c}{VE_o^2} \frac{d\Sigma}{d\eta} . \tag{21}$$

The normalized quantity $d\Sigma/d\eta = 2\int_{\eta}^{\infty} p^*E^*\frac{d\sigma^*}{d\eta} F(p^*)dp^*$, which has the dimensions of a cross section (recall p^* and E^* are measured in electron masses), is useful for comparing the effect in different storage rings. It is plotted as a function of η in Fig. 3, for unpolarized and fully polarized electrons; we have used a Gaussian function $F(p^*)$, for several typical values of δp^*. As expected, $d\Sigma/d\eta$ is a very rapidly decreasing function of η. The polarization-dependence can be seen clearly in Fig. 4 where the normalized difference $(d\Sigma_{unpol}/d\eta - d\Sigma_{pol}/d\eta)/d\Sigma_{unpol}/d\eta$ is plotted as a function of η.

Consider an experiment to detect the outscattered electrons with an acceptance limited to a small bite $\Delta\eta$. Using equation (21) we have

$$\frac{dW}{dt} = \frac{N^2c}{VE_o^2} \frac{d\Sigma}{d\eta} \Delta\eta . \tag{22}$$

For such an experiment Table I gives the values of the various machine-dependent parameters as we have estimated them for SPEAR (see the Appendix), together with the resulting counting rates, eq. (22), and the size of the polarization-dependent effect for several salient values of η. In going from dW/dt (instantaneous) to dW/dt (ave.) we have included an estimated duty factor of .03, corresponding to the fraction of time per turn that an electron spends in the region being observed. The last column in Table I shows the statistical error on the difference $(dW_{unpol} - dW_{pol})dW_{unpol}$ for

data accumulated over a 1000 second interval.

From the numbers in Table I we conclude that a Touschek effect experiment has reasonable promise as a means of detecting and monitoring the polarization of the electrons in SPEAR, at least at 2.5 GeV. Although the polarization-dependent effect is small, the counting rates are high enough to provide good statistical precision. We envision an experimental arrangement at SPEAR that would select scatterings at $\eta \simeq .05$, with counting rates of the order of tens per second at a luminosity of 0.2×10^{32} cm^2 sec^{-1}. The chief virtue of the method is that the presence of polarizations of the expected magnitude can be detected with data accumulated over a few hours, which makes it possible to investigate the effects of different running conditions or to monitor the polarization during longer experiments with colliding beams.

We should point out that these results become somewhat less favorable as the energy of the storage ring is increased. The counting rates fall as $E_o^{-5.5}$, taking into account both the explicit E_o^{-2} dependence of equation (22) and the variation of the beam volume with energy (equation (A-2). Also the width of the radial momentum distribution increases as E_o^2 (equation A-5), causing dilution of the polarization-dependent effect. Tending to offset these difficulties is the fact that the polarization buildup time decreases as E_o^{-5} (equation (3)).

An experiment similar to the one we have just described has been carried out at the ACO (Orsay) storage ring.[8] A net decrease of 19% was observed in the scattering rate at $t = T_{ACO}$, in agreement with the calculated value for ACO of 22%. In that experiment the counters were placed to accept events at $\eta = .07$. Fig. 4 yields a net effect of about 22% for $\delta p_\perp \simeq 0.15$ MeV.[10]

E_o (GeV)	N	V (cm^3)	$\delta p_\perp = \sqrt{2}\delta p^*$ (MeV)	$\Delta\eta$	η	$d\Sigma/d\eta$	dW/dt instantaneous (sec^{-1})	dW/dt ave. (sec^{-1})	$\frac{dW_{unpol}-dW_{pol}}{dW_{unpol}}$ ($\|P_1\|$ $\|P_2\|$=.85)	stat. error (1000 sec.)
2.5	6.4×10^{11}	1.6	0.6	0.005	0.05	7.5×10^{-21}	1.1×10^{4}	330.	0.056	± 0.002
					0.1	7.6×10^{-22}	1.1×10^{3}	33.	0.071	± 0.008
					0.2	7.3×10^{-23}	110	3.3	0.104	± 0.02
					0.3	1.7×10^{-23}	26	0.8	0.135	± 0.05

Table I. Counting rates and magnitude of the polarization dependence for specified storage ring parameters and detector acceptances. The instantaneous count rate dW/dt has been multiplied by a duty factor to obtain the average dW/dt. The statistical errors listed in the last column are based upon the number of counts recorded in a 1000-second interval.

It is also useful to consider what happens if instead of counting scattered electrons within a narrow band $\Delta\eta$ around η (differential counting), one includes all events with η greater than some minimum value (integral counting). The calculation for this case yields the total rate at which electrons are lost from the ring due to the Touschek effect, which is the case considered by Völkel[5] and Baier.[1] For the integral rate the analogue of eq. (16) is

$$\frac{dW}{dt}(p^*) = \frac{N^2 c}{V E_o^2} F(p^*)\, p^* E^* \sigma^*(p^*, \eta) , \tag{23}$$

where $\sigma^*(p^*,\eta) = \int_{\eta}^{p^*/E^*} (d\sigma^*/d\eta')\, d\eta'$, the upper limit corresponds to $\cos\chi = 1$ in eq. (9), and $d\sigma^*/d\eta'$ is given by eq. (10). The result of the integration is

$$\sigma^* = \frac{\pi r_o^2}{2p^{*4}E^{*2}} \left\{ (1 + 2p^{*2})^2 \left(\left(\frac{p^*}{E^*\eta}\right)^2 - 1 \right) - (1 + 4p^{*2}) \ln \frac{p^*}{E^*\eta} + p^{*4} \left(1 - \frac{E^*\eta}{p^*}\right) \right.$$

$$\left. - P_1 P_2 \left[(1+3p^{*2}) \ln \frac{p^*}{E^*\eta} - \frac{1}{2} p^{*2} (1 + 2p^{*2}) \left(1 - \left(\frac{E^*\eta}{p^*}\right)^2\right) + p^{*2}(2 + p^{*2}) \left(1 - \frac{E^*\eta}{p^*}\right) \right] \right\} \tag{24}$$

For the unpolarized case ($P_1 P_2 = 0$), this result reduces to equation (6) of Völkel[5].

Corresponding to equation (20) for the differential rate we now have

$$\frac{dW}{dt}(\eta) = \frac{N^2 c}{V E_o^2} \, 2 \int_{\eta/\sqrt{1-\eta^2}}^{\infty} p^* E^* \sigma^* F(p^*) \, dp^* \tag{25}$$

$$\equiv \frac{N^2 c}{V E_o^2} \Sigma \quad . \tag{26}$$

The results for Σ, obtained by integrating (25) numerically, are given in Figs. 5 and 6. The integral curves of Fig. 6 for the magnitude of the polarization dependence differ only slightly from those of Fig. 4 for the differential function $d\Sigma/d\eta$. The reason is that, because of the steep fall of $d\Sigma/d\eta$ with η (Fig. 3), the integral $\int_{\eta}^{1} d\Sigma/d\eta' \, d\eta'$ is dominated by contributions near $\eta' = \eta$.

Völkel[5] and Baier[1] have carried out the integration for Σ analytically for both square and Gaussian distributions in the approximation $\eta \ll 1$. The resulting formula for the Gaussian spectrum is[1,5]

$$\frac{dW}{dt} = \frac{2\pi \, r_o^2 \, c \, N^2}{V E_o^2 \, \eta_1^2} \cdot J \quad , \tag{27}$$

$$J = \frac{1}{2\sqrt{\pi}\,\delta p} \left(\ell n \frac{2}{\eta} - \frac{7}{4} - \frac{P_1 P_2}{4} \right) + \left(1 + \frac{1}{2(\delta p_\perp)^2} \right) e^{-\delta p_\perp^2} \left(1 - \Phi\left(\frac{1}{\delta p_\perp}\right) \right)$$

$$- \frac{1}{2\delta p_\perp} \int_o^{\frac{1}{\delta p_\perp}} d x \, e^{x^2} \left(1 - \Phi(x) \right) \quad , \tag{28}$$

where $\Phi(x)$ is the error function. This is equation (5.13) in reference 1 with a factor of 1/2 multiplying the right hand side. The factor 1/2 is included because Baier's eq. (5.13) refers to the rate at which electrons are lost from the beam, and two electrons are lost for each scattering[5]; our version, eq. (25), specifies the scattering event rate. Using eq. (27)

the function Σ defined by eq. (26) is given by

$$\Sigma = \frac{2\pi\, r_o^2}{\eta^2} \cdot J \tag{29}$$

Finally, the expression for J may be expanded in a power series[5] in $1/\delta p_\perp$:

$$J = 1 + \frac{1}{2\sqrt{\pi}\,\delta p_\perp}\left(\ln\frac{2}{\eta} - \frac{23}{4} - \frac{P_1 P_2}{4}\right)$$

$$+ \sum_{n=0}^{\infty}\left(\frac{1}{\delta p_\perp}\right)^{2n+2}\frac{1}{n!}\,\frac{n^2+3n+1}{2n^2+3n+1} - \frac{1}{\sqrt{\pi}}\sum_{n=0}^{\infty}\left(\frac{1}{\delta p_\perp}\right)^{2n+3}\frac{2^n}{(2n+1)!!}\,\frac{n^2+4n+2.75}{n^2+2.5n+1.5} \tag{30}$$

The results of evaluating formulas (29) and (30) are included in Figs. 5 and 6 for comparison with our results. The two calculations agree well in the limit $\eta \ll 1$, i.e., where the approximation used in references 1 and 5 is valid. In Fig. 6, the value of $\Sigma_{unpol} - \Sigma_{pol}/\Sigma_{unpol} = 0.055$ for $\eta \geq 0.01$ and $\delta p_\perp = .5$ MeV agrees with the value of 0.06 given by Baier[1] (p. 41), corresponding to the Novosibirsk Storage ring VEPP-2.

III. Alternative methods to measure the polarization of e^-e^+ beams in storage rings.

In the previous section it has been shown that the polarization of an $e^-(e^+)$ beam in a storage ring can be observed by detecting pairs of electrons which have gone through large angle Coulomb scattering initiated by the radial betatron oscillations within a bunch. The rate for detecting such pairs of electrons lost due to this so-called Touschek effect depends on the transverse polarization of the electrons. Hence one might expect to observe the counting rate to decrease with time as the polarization slowly builds up.[8] For SPEAR running at 2.5 GeV, for example, we have

shown that there is a 5-10% difference in the outscattered counting rate between a polarized and non-polarized beam, for admissible values of the fractional energy exchange of the scattered electrons in the laboratory. It is also of interest to investigate other, possibly more direct, methods of searching for evidence of $e^-(e^+)$ polarization that might confirm a Touschek scattering experiment and also provide additional physical information.

In this section, we discuss the angular distributions of three e^+e^- collision processes which normally are azimuthally symmetric but which show azimuthal (φ) asymmetry when the e^+, e^- beams are polarized. Experiments observing such asymmetry would provide unequivocal, independent evidence of beam polarization, and possess high intrinsic interest in their own right.

We consider the processes i) $e^+e^- \to \mu^+\mu^-$, ii) $e^+e^- \to e^+e^-$ and iii) $e^+e^- \to \gamma\gamma$, for which the differential cross-sections with polarized e^+e^- beams are given by[1]

$$\frac{d\sigma}{d\Omega}(e^+e^- \to \mu^+\mu^-) = \frac{r_o^2}{16\gamma^2}\beta_\mu\left\{2-\beta_\mu^2\sin^2\theta\left[1+|\vec{P}_1||\vec{P}_2|\,(2\sin^2\varphi-1)\right]\right\}, \tag{31}$$

$$\frac{d\sigma}{d\Omega}(e^+e^- \to e^+e^-) = \frac{r_o^2}{16\gamma^2}\left(\frac{3+\cos^2\theta}{1-\cos\theta}\right)^2\left[1+\frac{|\vec{P}_1||\vec{P}_2|\sin^4\theta}{(3+\cos^2\theta)^2}(1-2\sin^2\varphi)\right], \tag{32}$$

$$\frac{d\sigma}{d\Omega}(e^+e^- \to \gamma\gamma) = \frac{r_o^2}{4\gamma^2(1-\beta_e^2\cos^2\theta)}\left[1+\cos^2\theta+|P_1||P_2|\sin^2\theta\,(1-2\sin^2\varphi)\right], \tag{33}$$

where θ is the scattering angle, φ is the angle between the production plane and the plane normal to the polarization vector (the azimuthal angle), $|P_1|$, $|P_2|$ is the magnitude of polarization of electrons and positions, $\gamma = E_o/m_e$ with E_o the energy of each of the e^+, e^- beams, β_μ, β_e are the velocities of $\mu^+(\mu^-)$ and $e^+(e^-)$ and r_o is the classical electron radius.

We observe in the above equations that there is azimuthal asymmetry in the angular distributions of the outgoing particles proportional to the beam polarizations. In all three processes, the asymmetry is maximal at $\theta = \pi/2$. The degree of asymmetry in the process $e^+e^- \to e^+e^-$ is smallest because the term which depends on polarization is reduced by a factor of 1/9.

The differential cross-sections for these processes are shown in Figure 7-12. In Figures 7-9 are plotted $\frac{d\sigma}{d\Omega}$ vs θ, the scattering angle, for $\varphi = \pi/2$ while Figures 10-12 contain $\frac{d\sigma}{d\Omega}$ vs φ for $\theta = \pi/2$. It is expected that the magnitude of the e^+,e^- polarizations will increase with time according to equation (2), $P(t) = P_o(1-e^{-t/T})$, where it is assumed that the storage ring is completely filled at $t = 0$. We have therefore plotted the differential cross-sections for different values of $< P^2(t) >$ defined by

$$< P^2(t) > \equiv \frac{1}{t_2-t_1} \int_{t_1}^{t_2} P_o(1-e^{-t/T})^2 \, dt. \qquad (34)$$

The values of $< P^2(t) >$ are obtained by allowing t_1 to vary and taking $t_2 = 4$ hrs., i.e., approximately twice the nominal beam lifetime at SPEAR. The time constant T is a strongly energy dependent quantity. At SPEAR, it is estimated that $T \simeq 165\text{hr}/E_o^5$ (GeV). All the curves for $\frac{d\sigma}{d\Omega}$ are plotted by taking $E_o = 2.5$ GeV. We have also plotted the differential cross-sections for the cases $|\vec{P}_1| = |\vec{P}_2| = 0$ and $|\vec{P}_1| = |\vec{P}_2| = P_o$ (=0.924) for comparison.

In order to compare quantitatively the sensitivity of each of the three processes to the polarization we have calculated also the percentage statistical error on $< P^2(t) >$, viz, $\Delta<P^2>/<P^2>$, which would be obtained in a measurement of $\frac{d\sigma}{d\Omega}$ in the angular region $85^\circ \leq \theta \leq 95^\circ$ and

$0^\circ \leq \varphi \leq 180^\circ$; this is done as a function of net data collecting time for different values of $< P^2 >$, assuming that the luminosity is 2×10^{31} cm^{-2} sec^{-1} for $E_o = 2.5$ GeV. The results are shown in Figures 13-15 from which one sees that both $e^+e^- \rightarrow \mu^+\mu^-$ and $e^+e^- \rightarrow \gamma\gamma$ yield relatively precise determinations of $< P^2 >$ for moderate data collecting time, even for $< P^2 > = 0.38$.

To obtain the actual machine time that would be required, it is necessary only to multiply the abscissa for each of the curves of Figures by the factor $t_2/(t_2-t_1)$. This is done explicitly for the case $e^+e^- \rightarrow \mu^+\mu^-$ as shown in Figure 16 where the abscissa is total machine time. For a given total machine time, the error $\Delta<P^2>/< P^2>$ does not vary much with t_1, which means that the point in time at which data-taking starts is not critical. For 300 hours of total machine time, for example, a value of $\Delta< P^2>/< P^2> < 0.1$ is possible in a realistic experiment.

There is another possible method [1] for determining beam polarization in a storage ring, namely backward Compton scattering of circularly polarized laser photons from one of the circulating charged beams. We have not explored this alternative in detail because of the apparent promise of the Touschek effect and the e^+e^- collision experiments. This promise indicates that an experimental effort to study beam polarization and its consequences at SPEAR would be profitable. Such an effort, if successful, would lead directly to studies of second order QED effects and weak interactions [2] at an improved SPEAR of higher energy.

Appendix: Estimates of Storage Ring Parameters.

For the number of electrons in the bunch at SPEAR we have assumed 10^{12} at 2 GeV (corresponding to the full design luminosity), and have scaled this number for 2.5 GeV according to $N = 10^{12}\ (2\ \text{GeV}/E)^2$. This gives 6.4×10^{11} at 2.5 GeV.

For the effective volume of the beam we use the definition (15) and assume a Gaussian density distribution:

$$\rho = \frac{N}{(2\pi)^{3/2}\sigma_x\sigma_y\sigma_z}\, e^{-\frac{1}{2}\left(\frac{x^2}{\sigma_x^2}+\frac{y^2}{\sigma_y^2}+\frac{z^2}{\sigma_z^2}\right)} ,$$

$$\int \rho^2 dV = \frac{N^2}{(4\pi)^{3/2}\sigma_x\sigma_y\sigma_z} .$$

Therefore

$$V = (4\pi)^{3/2}\sigma_x\sigma_y\sigma_z . \qquad \text{(A-1)}$$

The natural beam dimensions at SPEAR are given by the following relations[9]:

$$\sigma_x = .24\text{mm}\ E_o(\text{GeV})\ \sqrt{\beta_x/\beta_x^*}$$

$$\sigma_y = .017\text{mm}\ E_o(\text{GeV})\ \sqrt{\beta_y/\beta_y^*}$$

$$\sigma_z \simeq 3.4\text{cm}\ (E_o(\text{GeV}))^{3/2}.$$

Here $\beta_{x,y}$ are the radial and vertical beta functions evaluated at the location in the ring where the observed scatterings occur, $\beta^*_{x,y}$ are the beta functions at the interaction regions: $\beta_x^* = 1.0\text{m}$, $\beta_y^* = 0.39\text{m}$. We have ignored a slight correction to σ_z which depends on the RF voltage.

$$V = (4\pi)^{3/2} \times 1.39 \times 10^{-4} \; (E_o(\text{GeV}))^{7/2} \sqrt{\beta_x \beta_y / \beta_x^* \beta_y^*} \qquad \text{(A-2)}$$

If the source of events is a standard straight section, where $\beta_x = 14.2\text{m}$, $\beta_y = 3.0\text{m}$, and $E_o = 2.5$ GeV, then $V = 1.6$ cm^3.

The rms radial momentum $\delta p_\perp$ is

$$\delta p_\perp = E_o \sigma_x' \qquad \text{(A-3)}$$

with the angular divergence σ_x' related to the beta function by[9]

$$\sigma_x' = .24 \times 10^{-3} \text{m} \sqrt{\frac{1 + (\beta_x'/2)^2}{\beta_x^* \beta_x}} \; E_o(\text{GeV}) \qquad \text{(A-4)}$$

At a standard straight section the beam is parallel, i.e., $\beta_x' = 0$. With $\beta_x^* = 1$ m, $\beta_x = 14.2$ m we get

$$\delta p_\perp = .064 \; (E_o(\text{GeV}))^2 \times 10^{-3}, \qquad \text{(A-5)}$$

or $\delta p_\perp = 0.4$ MeV at 2.5 GeV. Elsewhere in the normal cells the value is $\delta p_\perp = 0.9$ MeV.

References

1. V. N. Baier, XLVI Corso Scuola International di Fizica "Enrico Fermi", 4 (1969). Academic Press.
2. See experimental proposal SP-7 submitted to SLAC by A. K. Mann, D. B. Cline and D. D. Reeder, unpublished. Also J. Godine and A. Hankey, MIT Center for Theoretical Physics, Publication No. 279 (to be published). A. Love, Rutherford Laboratory preprint RRP/T/11. V. K. Cung, A. K. Mann and E. A. Paschos, NAL preprint 68 (to be published).
3. C. Bernardini, et al. Phys. Rev. Letters 10, 407 (1963).
4. B. Gittleman and D. M. Ritson, Stanford Internal Report HEPL-291 (1963).

5. U. Völkel, DESY Report 67/5 (1967).

6. A. A. Kresnin and L. N. Rosenzweig, Soviet Physics JETP 5, 288 (1957).

7. A. I. Akhiezer and V. B. Berestetsky, Quantum Electrodynamics. Interscience Publishers, 1965, p. 505.

8. J. LeDuff, P. C. Marin, P. Petroff and E. Sommer, Proc. of the 1971 Symposium on Electron and Photon Interactions at High Energies, Cornell University, Ithaca, N. Y., 1971.

9. J. E. Augustin, private communication. It should be pointed out that when the machine is tuned to optimize the luminosity it is necessary to enlarge the beam beyond the natural dimensions assumed here. This would have the effect of lowering the Touschek counting rate.

10. Actually the calculation for ACO involves averaging the counting rates over the appropriate segment of the beam orbit where both η and $\delta p_\perp$ are functions of the azimuth (see J. Le Duff, ACO Internal Note 10-68).

    A very recent paper from ACO (unpublished) describes a new series of experiments showing that the expected polarization of the positron beam occurs even in the presence of a colliding electron beam. The earlier null result in $e^+e^- \to \mu^+\mu^-$ is now understood as the effect of a depolarizing resonance.

11. Resonance depolarization occurs if the energy of the storage ring satisfies the relation $\frac{E}{m}\left(\frac{g-2}{2}\right) = k \pm \nu_x \pm \nu_y$, $k = 0, 2, 4, \ldots$, where $\nu_{x,y}$ are the radial and vertical betatron wave numbers and k is an even integer in SPEAR because of the two-fold symmetry. (Private communication from R. Schwitters.) More difficult to calculate is the effect of stochastic depolarization (see ref. 1), which occurs at rates which increase with energy relative to the polarization

build up rate. Our rough estimate for SPEAR indicates that the effect is small.

Figure Captions

Figure 1. Definition of the center-of-mass angles θ, φ, x, ω. P_1 and P_2 are polarization vectors of the electrons.

Figure 2. The normalized counting rate $p^*E^*d\sigma^*/d\eta$ versus p^*, for selected fixed values of η.

Figure 3. $d\Sigma/d\eta = 2\int_{\eta}^{\infty} dp^*p^*E^* \frac{d\sigma^*}{d\eta} F(p^*)$ versus η. $F(p^*)$ is Gaussian, with standard deviation $\delta p^* = \delta p_\perp/\sqrt{2}$.

Figure 4. The normalized difference between counting rates with and without polarization, for differential counting, versus η.

Figure 5. $\Sigma = 2\int_{\eta}^{\infty} dp^*p^*E^*\sigma^*F(p^*)$ versus η. $F(p^*)$ is Gaussian, with standard deviation $\delta p^* = \delta p_\perp/\sqrt{2}$. The curve for $\delta p_\perp$ = 1 MeV from the formula of Völkel[5] is shown for comparison with our results.

Figure 6. The normalized difference between counting rates with and without polarization, for integral counting, versus η.

Fig. 7-9. Plots of $\frac{d\sigma}{d\Omega}^{(e^+e^- \to \mu^+\mu^-)}$, $\frac{d\sigma}{d\Omega}^{(e^+e^- \to e^+e^-)}$, $\frac{d\sigma}{d\Omega}^{(e^+e^- \to \gamma\gamma)}$ versus scattering angle φ for $\theta = \pi/2$ for different values of

$$\langle p^2 \rangle = \frac{1}{t_2 - t_1} \int_{t_1}^{t_2} p_o^2 (1 - e^{-t/T})^2 dt.$$

The meaning of the label on each of the curves is explained by the following table:

Label on curve	t_1(hr.)	$\langle P^2 \rangle$
a		$0 (P_1 = P_2 = 0)$
b	0.0	0.38
c	0.8	0.47
d	1.6	0.55
e	2.4	0.61
f	3.2	0.67
g		$0.85 (P_1 = P_2 = 0.924)$

Figure 10-12. Plots of $\frac{d\sigma}{d\Omega}(e^+e^- \to \mu^+\mu^-)$, $\frac{d\sigma}{d\Omega}(e^+e^- \to e^+e^-)$, $\frac{d\sigma}{d\Omega}(e^+e^- \to \gamma\gamma)$ versus θ for $\varphi = \pi/2$, for different values of $\langle P^2 \rangle$.

Figure 13-15. Plots of $\Delta\langle P^2 \rangle / \langle P^2 \rangle$, for processes $e^+e^- \to \mu^+\mu^-$, $e^+e^- \to e^+e^-$, $e^+e^- \to \gamma\gamma$, versus net data collecting time for different values of $\langle P^2 \rangle$.

Figure 16. Plot of $\Delta\langle P^2 \rangle / \langle P^2 \rangle$, for reaction $e^+e^- \to \mu^+\mu^-$, versus total machine time required for different values of $\langle P^2 \rangle$.

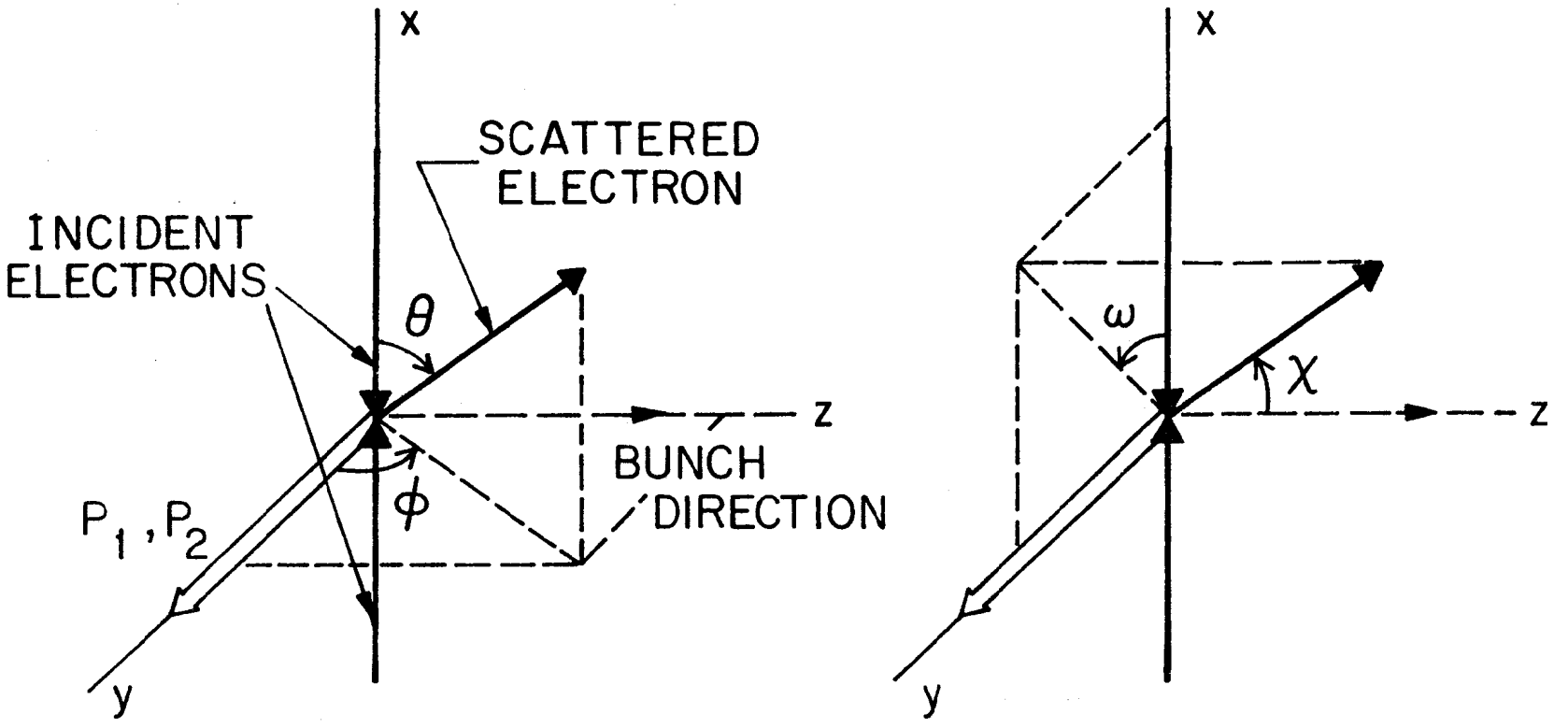
x
SCATTERED
ELECTRON
INCIDENT
ELECTRONS
θ
z
BUNCH
DIRECTION
φ
P1, P2
y
x
ω
χ
z
y

Fig. 1

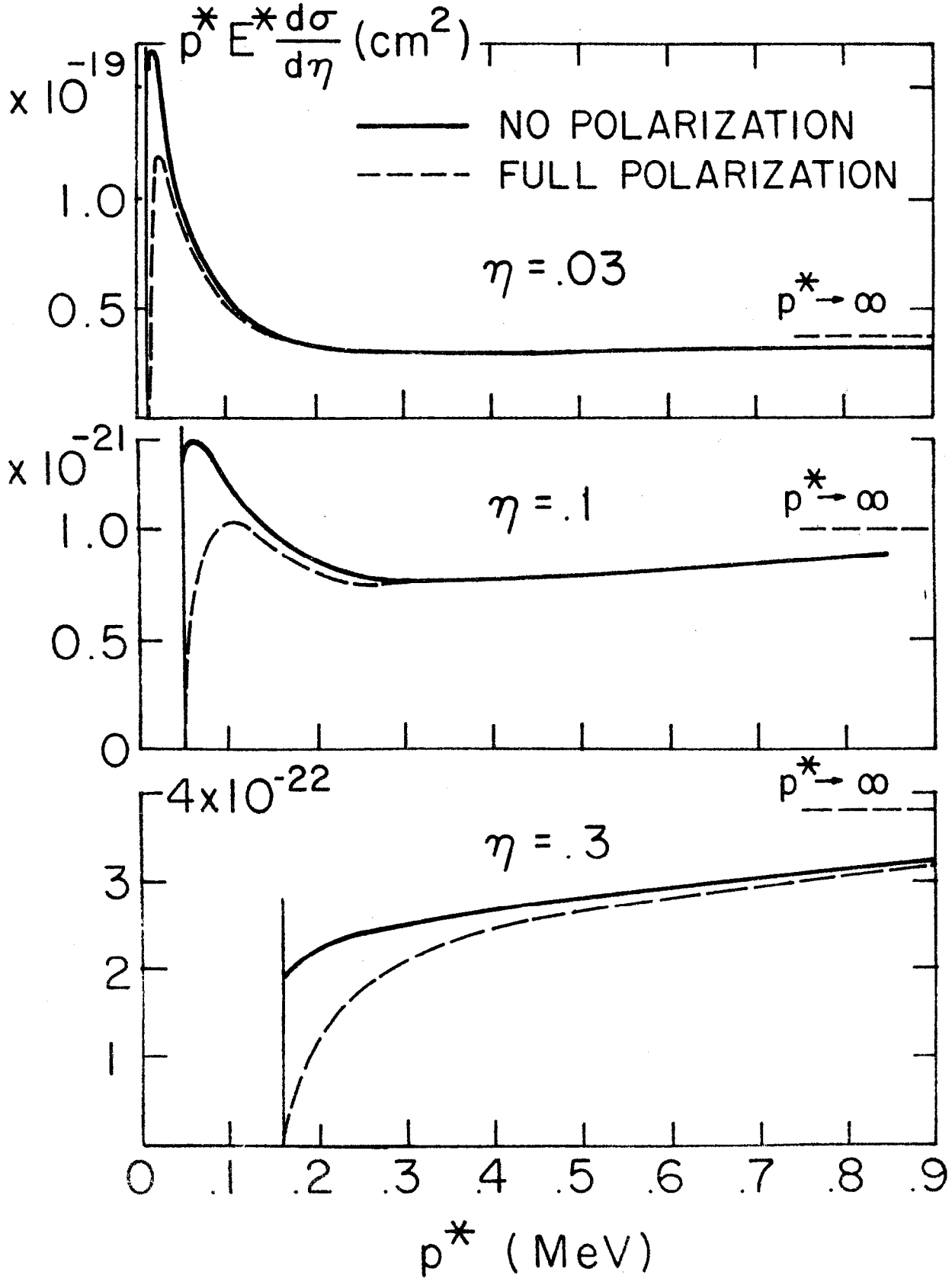
$p^* E^* \frac{d\sigma}{d\eta}$ (cm^2)
x 10^{-19}
1.0
0.5
NO POLARIZATION
FULL POLARIZATION
η = .03
$p^* \to \infty$
x 10^{-21}
1.0
0.5
0
η = .1
$p^* \to \infty$
4x10^{-22}
3
2
1
η = .3
$p^* \to \infty$
0 .1 .2 .3 .4 .5 .6 .7 .8 .9
p^* (MeV)

Fig. 2

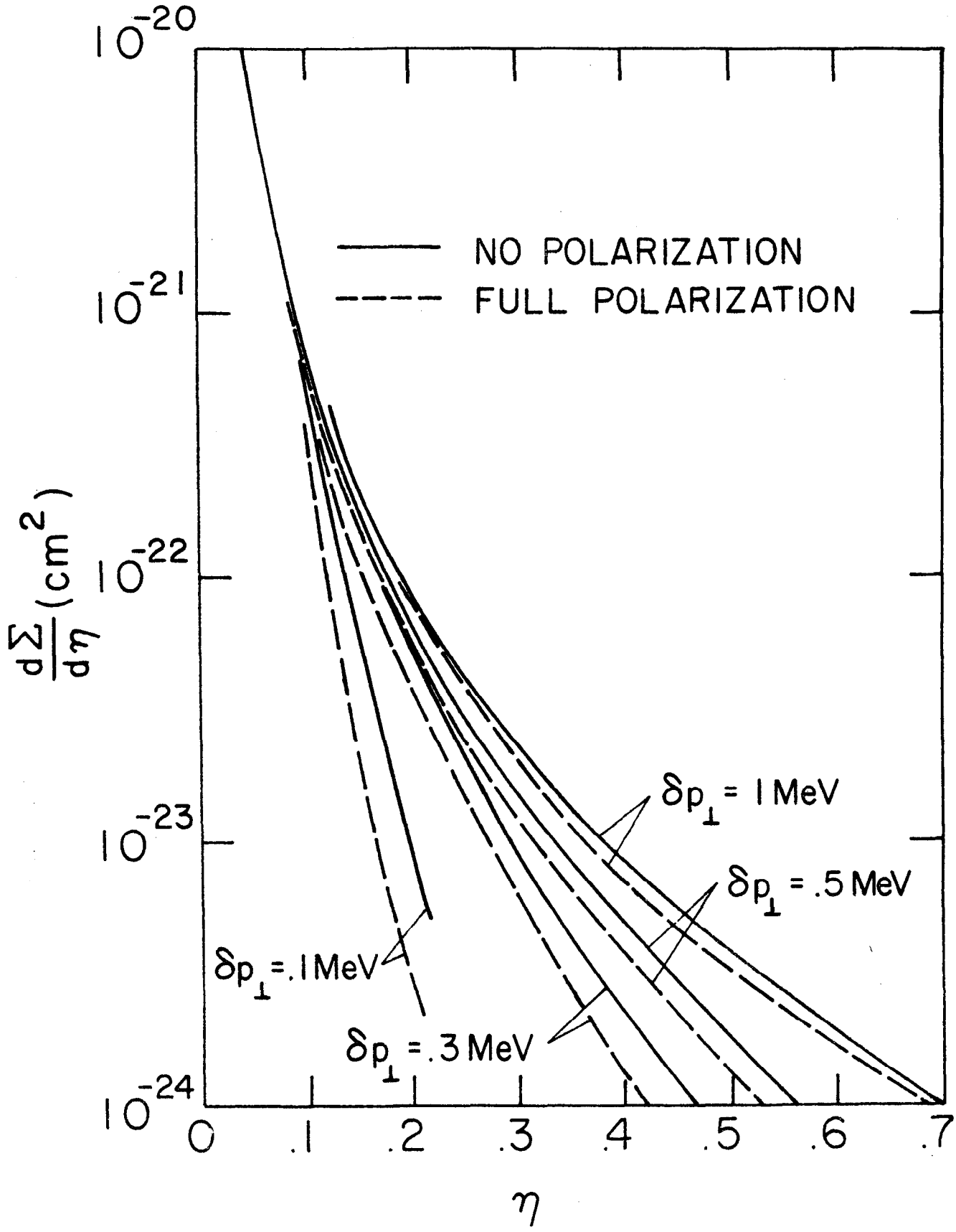
10^{-20}
10^{-21}
10^{-22}
10^{-23}
10^{-24}
$\frac{d\Sigma}{d\eta}(cm^2)$
NO POLARIZATION
FULL POLARIZATION
$\delta p_\perp$ = 1 MeV
$\delta p_\perp$ = .5 MeV
$\delta p_\perp$ = .3 MeV
$\delta p_\perp$ = .1 MeV
0
.1
.2
.3
.4
.5
.6
.7
η

Fig. 3

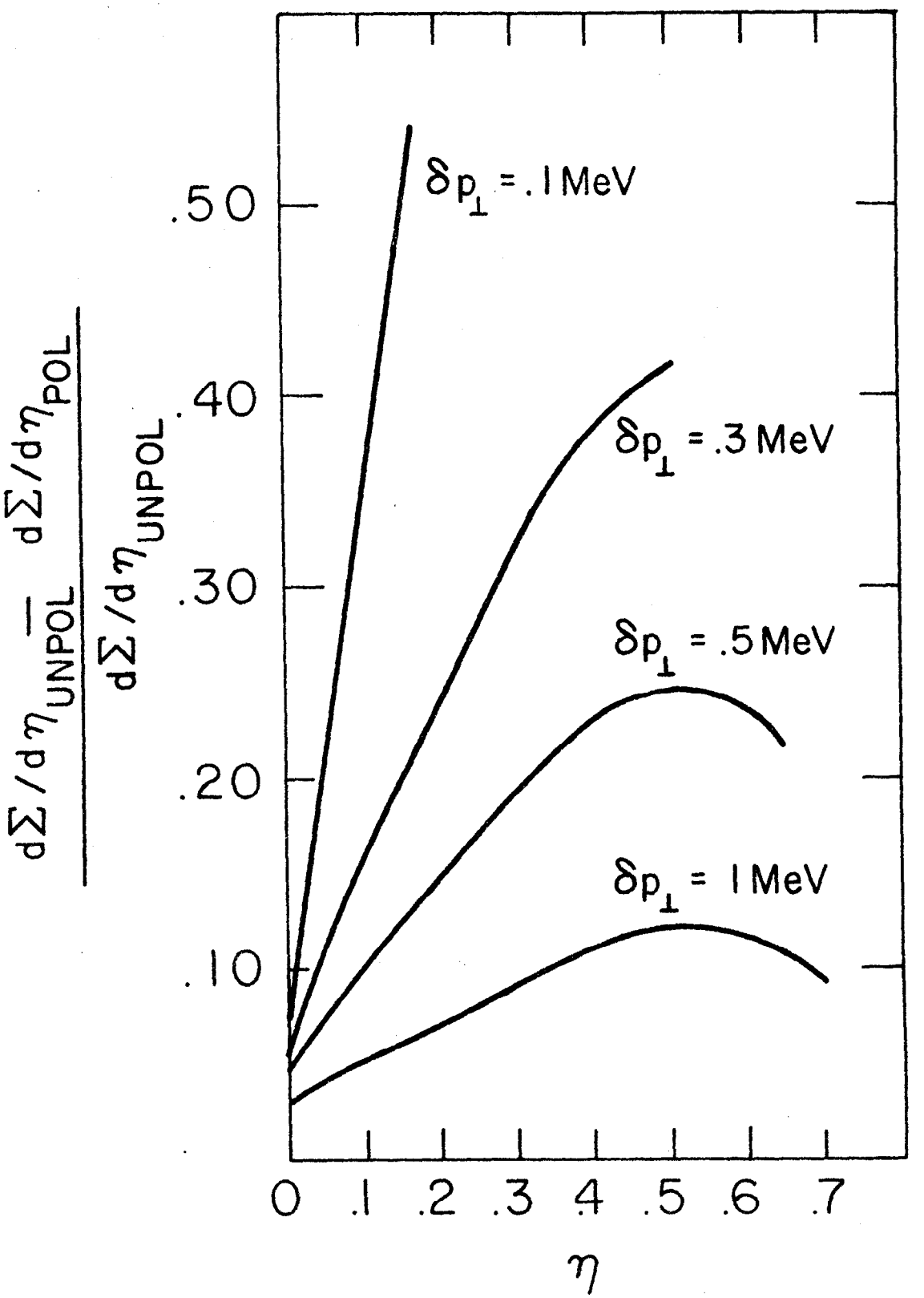
$\frac{d\Sigma/d\eta_{UNPOL} - d\Sigma/d\eta_{POL}}{d\Sigma/d\eta_{UNPOL}}$
.50
.40
.30
.20
.10
$\delta p_\perp$ = .1 MeV
$\delta p_\perp$ = .3 MeV
$\delta p_\perp$ = .5 MeV
$\delta p_\perp$ = 1 MeV
0 .1 .2 .3 .4 .5 .6 .7
η

Fig. 4

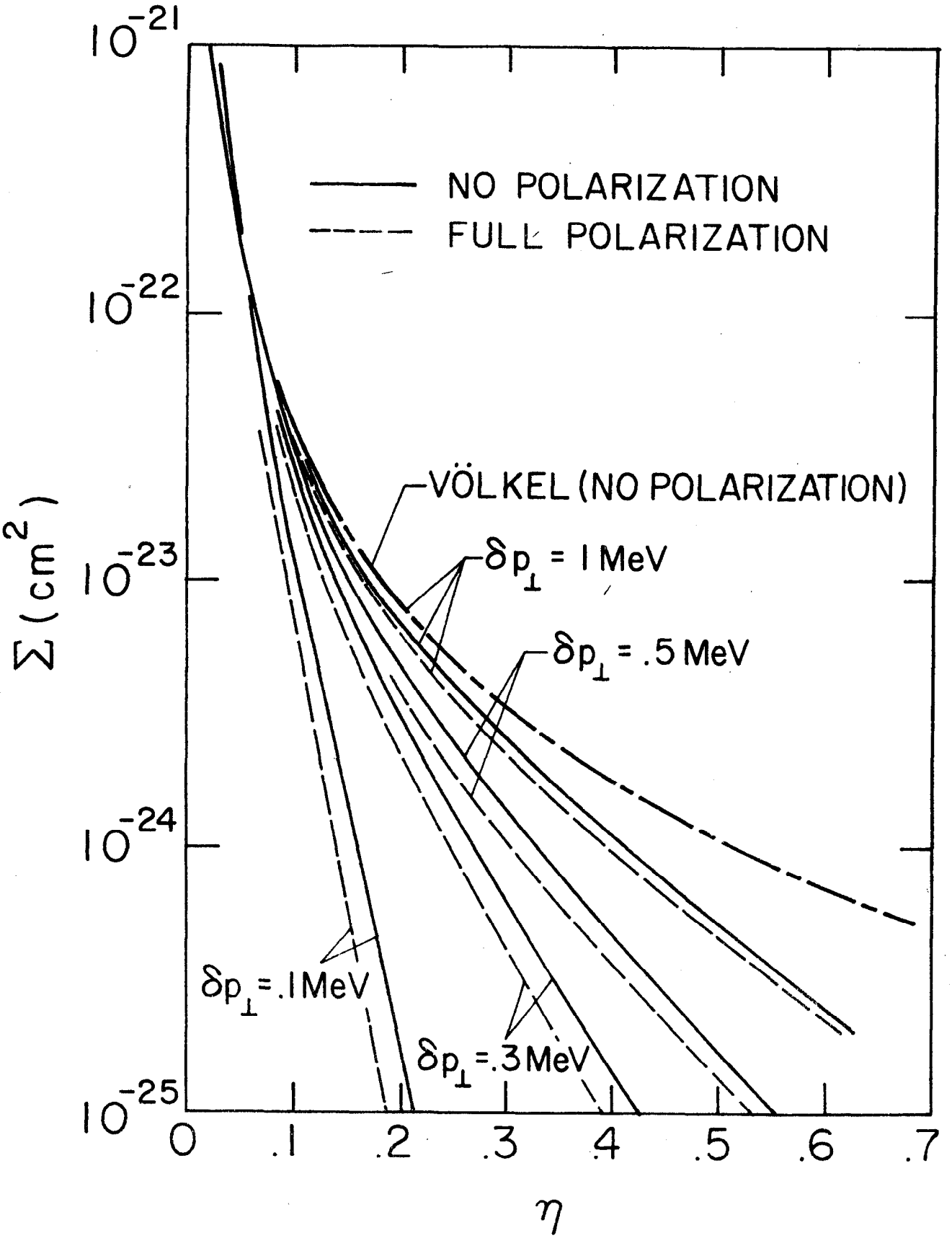
10^{-21}
10^{-22}
10^{-23}
10^{-24}
10^{-25}
$\Sigma\,(cm^2)$
NO POLARIZATION
FULL POLARIZATION
VÖLKEL (NO POLARIZATION)
$\delta p_\perp$ = 1 MeV
$\delta p_\perp$ = .5 MeV
$\delta p_\perp$ = .1 MeV
$\delta p_\perp$ = .3 MeV
0
.1
.2
.3
.4
.5
.6
.7
η

Fig. 5

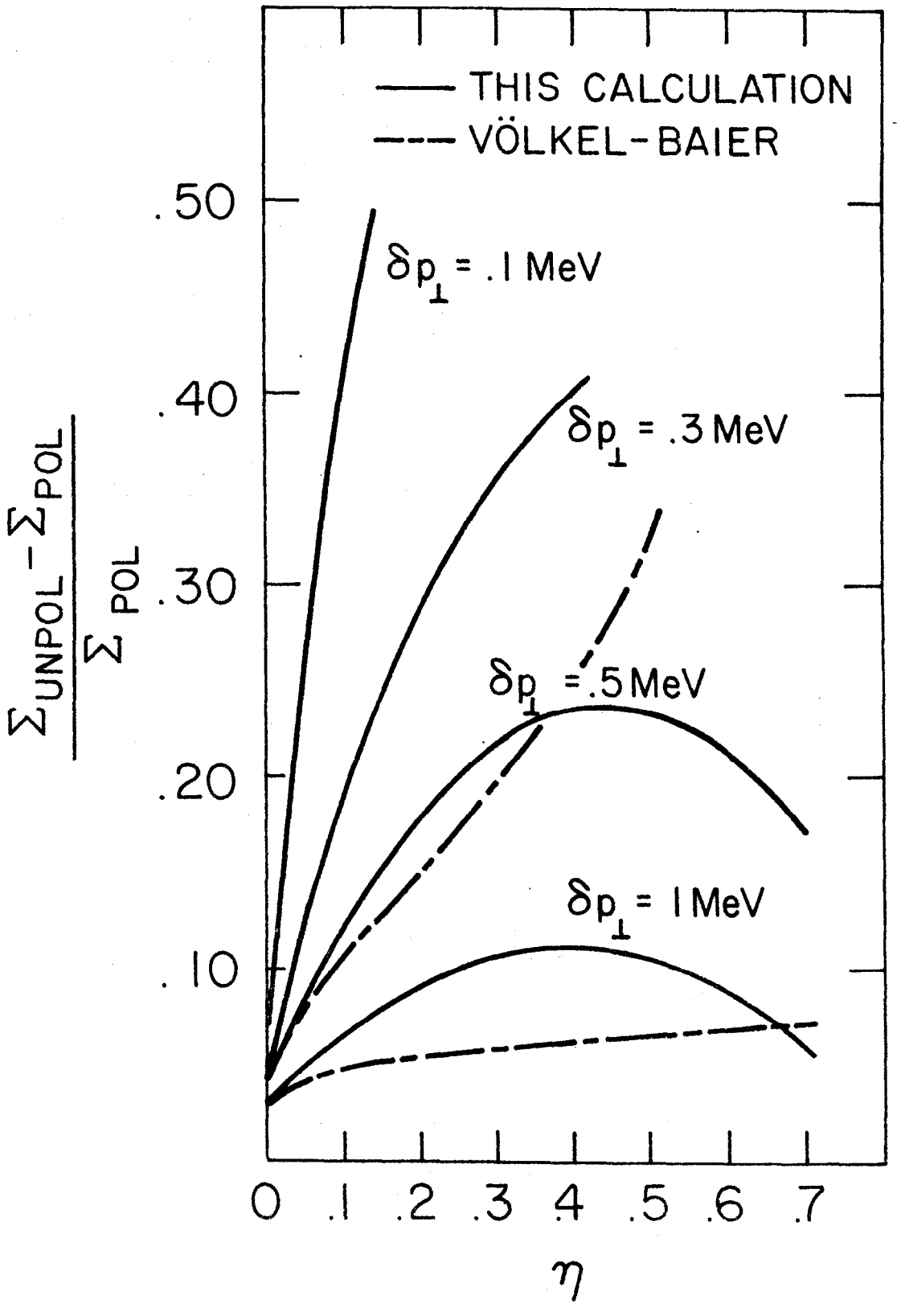
THIS CALCULATION
VÖLKEL-BAIER
$\delta p_\perp$ = .1 MeV
$\delta p_\perp$ = .3 MeV
$\delta p_\perp$ = .5 MeV
$\delta p_\perp$ = 1 MeV
$\frac{\Sigma_{UNPOL} - \Sigma_{POL}}{\Sigma_{POL}}$
.50
.40
.30
.20
.10
0
.1
.2
.3
.4
.5
.6
.7
η

Fig. 6

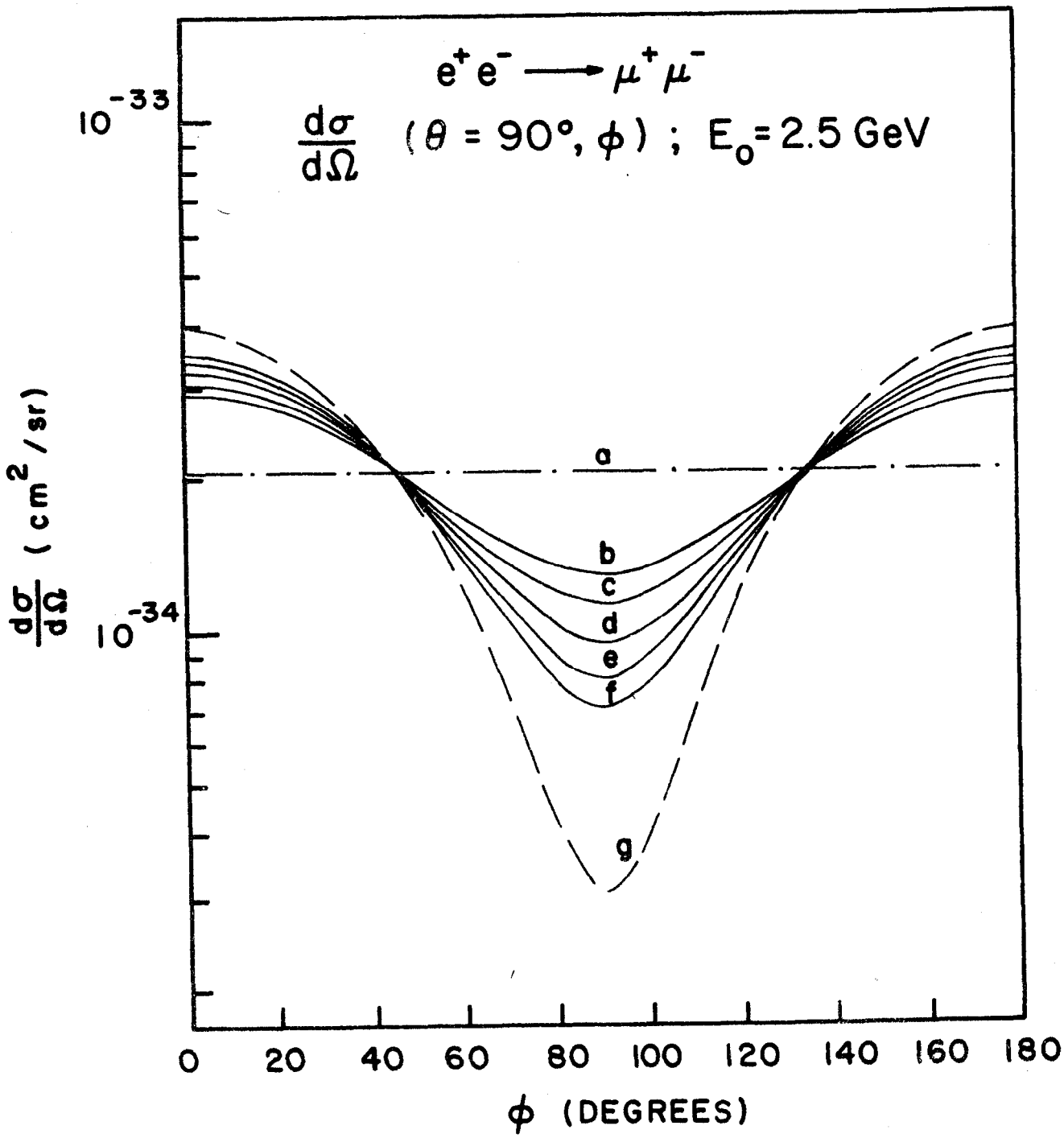
$e^+e^- \longrightarrow \mu^+\mu^-$
$\frac{d\sigma}{d\Omega}$ $(\theta = 90°, \phi)$; $E_0 = 2.5$ GeV
10^{-33}
10^{-34}
$\frac{d\sigma}{d\Omega}$ (cm^2 / sr)
a
b
c
d
e
f
g
0 20 40 60 80 100 120 140 160 180
ϕ (DEGREES)

Fig. 7

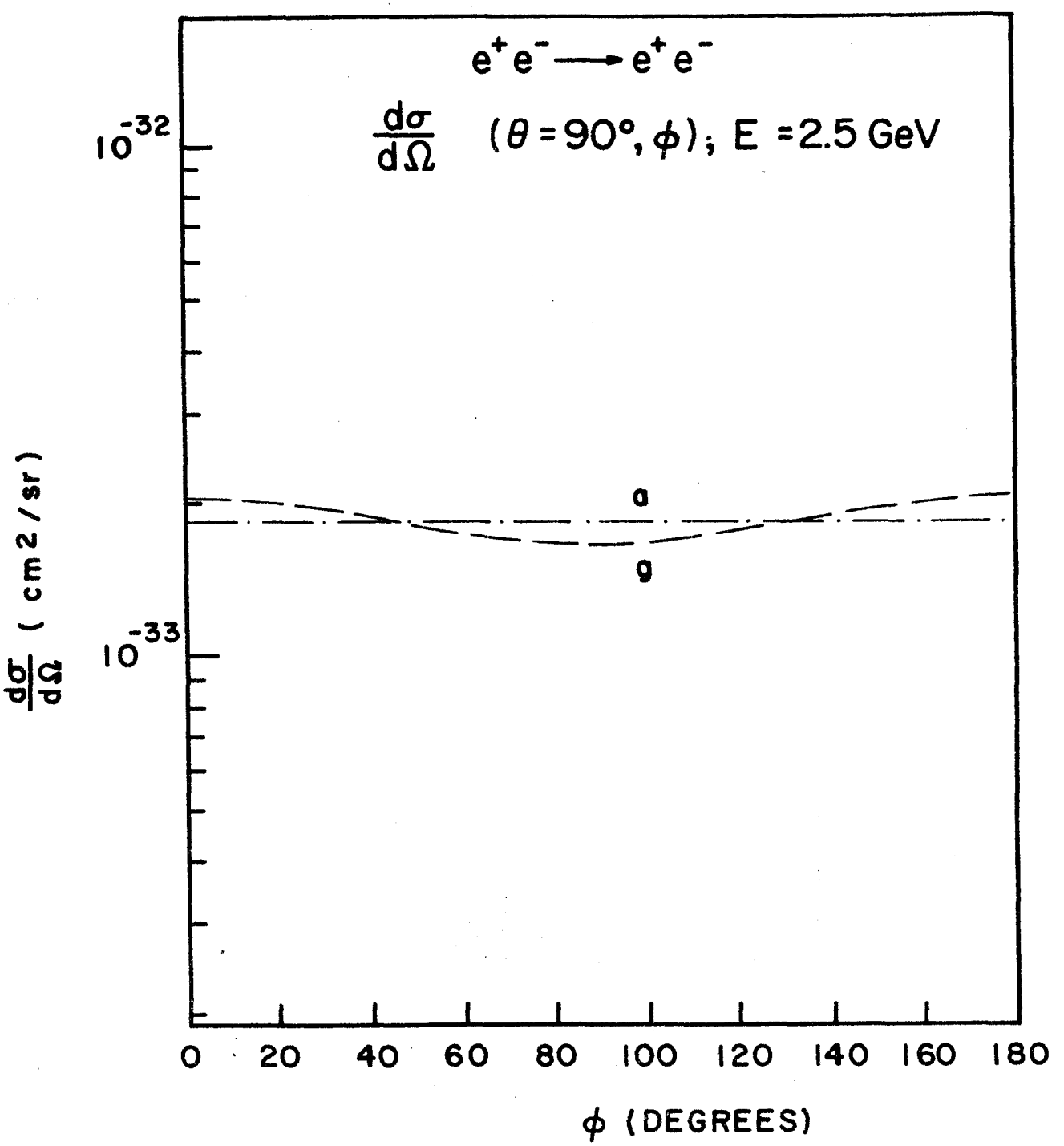
$e^+e^- \longrightarrow e^+e^-$
$\frac{d\sigma}{d\Omega}$ $(\theta = 90°, \phi)$; E = 2.5 GeV
10^{-32}
10^{-33}
a
g
$\frac{d\sigma}{d\Omega}$ (cm2 / sr)
0 20 40 60 80 100 120 140 160 180
ϕ (DEGREES)

Fig. 8

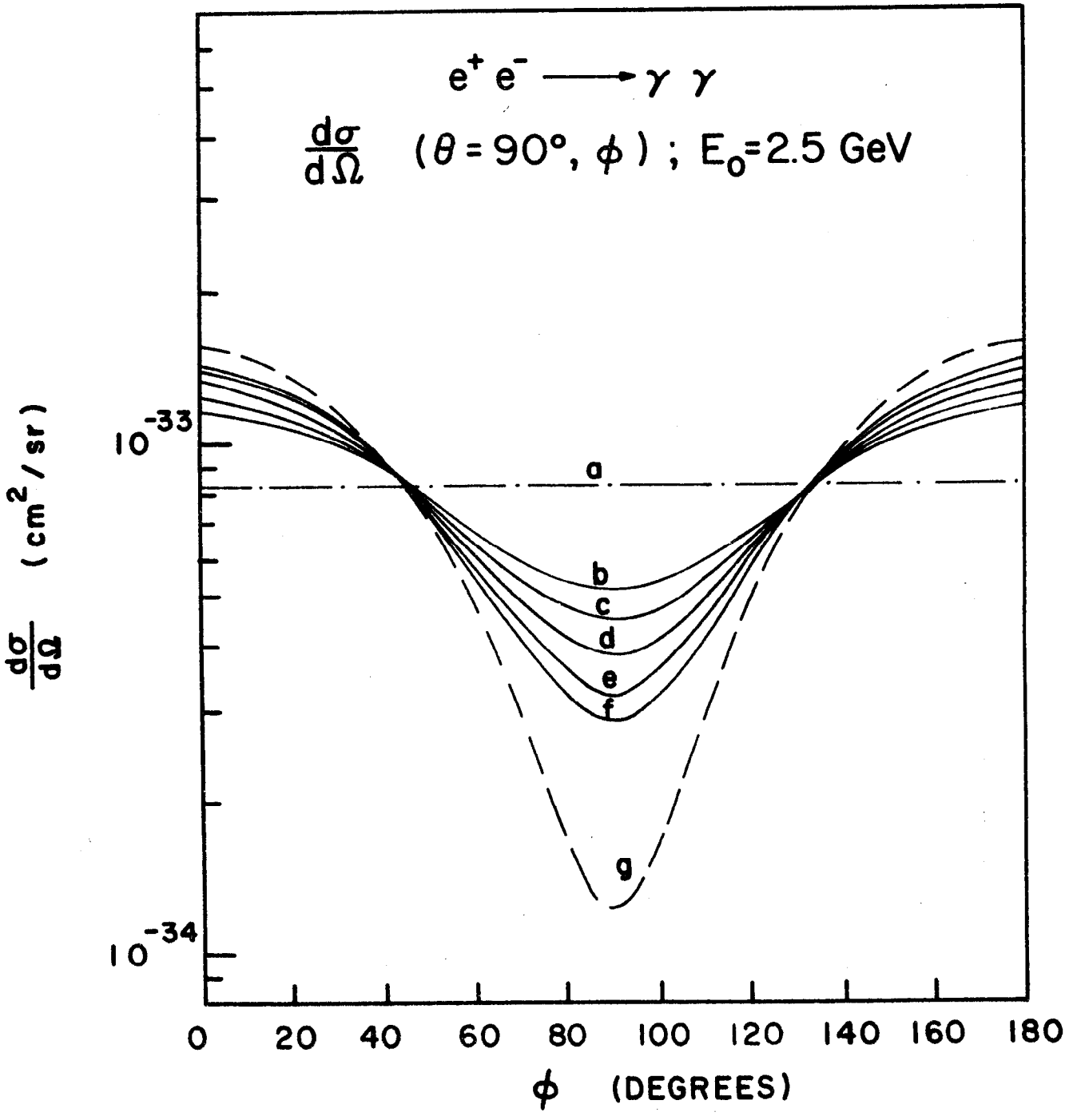
$e^+ e^- \longrightarrow \gamma\ \gamma$
$\frac{d\sigma}{d\Omega}$ $(\theta = 90°, \phi)$; E_0=2.5 GeV
$\frac{d\sigma}{d\Omega}$ (cm^2 / sr)
10^{-33}
10^{-34}
a
b
c
d
e
f
g
0 20 40 60 80 100 120 140 160 180
ϕ (DEGREES)

Fig. 9

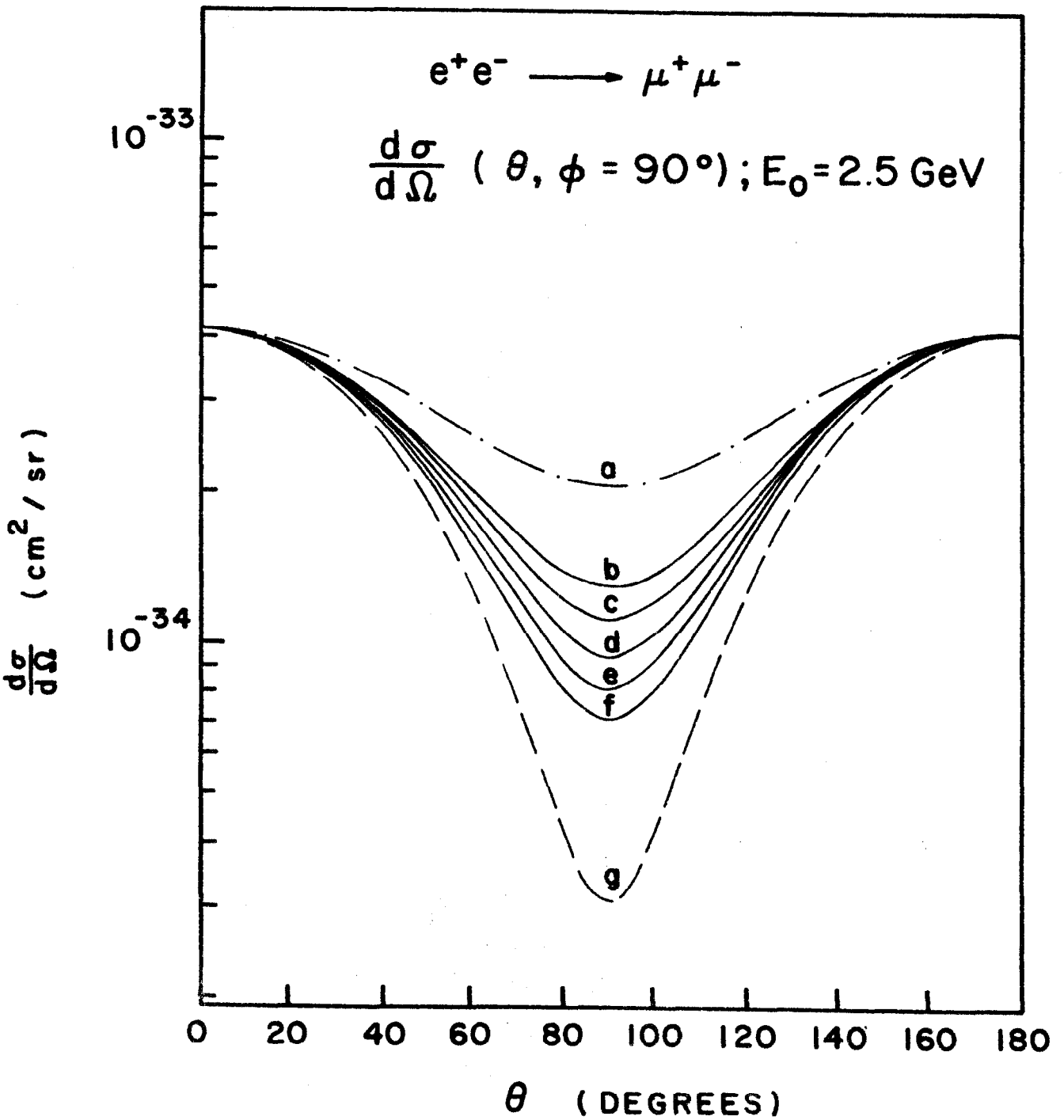
$e^+e^- \longrightarrow \mu^+\mu^-$
$\frac{d\sigma}{d\Omega}$ (θ, ϕ = 90°); E_0 = 2.5 GeV
10^{-33}
10^{-34}
$\frac{d\sigma}{d\Omega}$ (cm^2 / sr)
a
b
c
d
e
f
g
0
20
40
60
80
100
120
140
160
180
θ (DEGREES)

Fig. 19

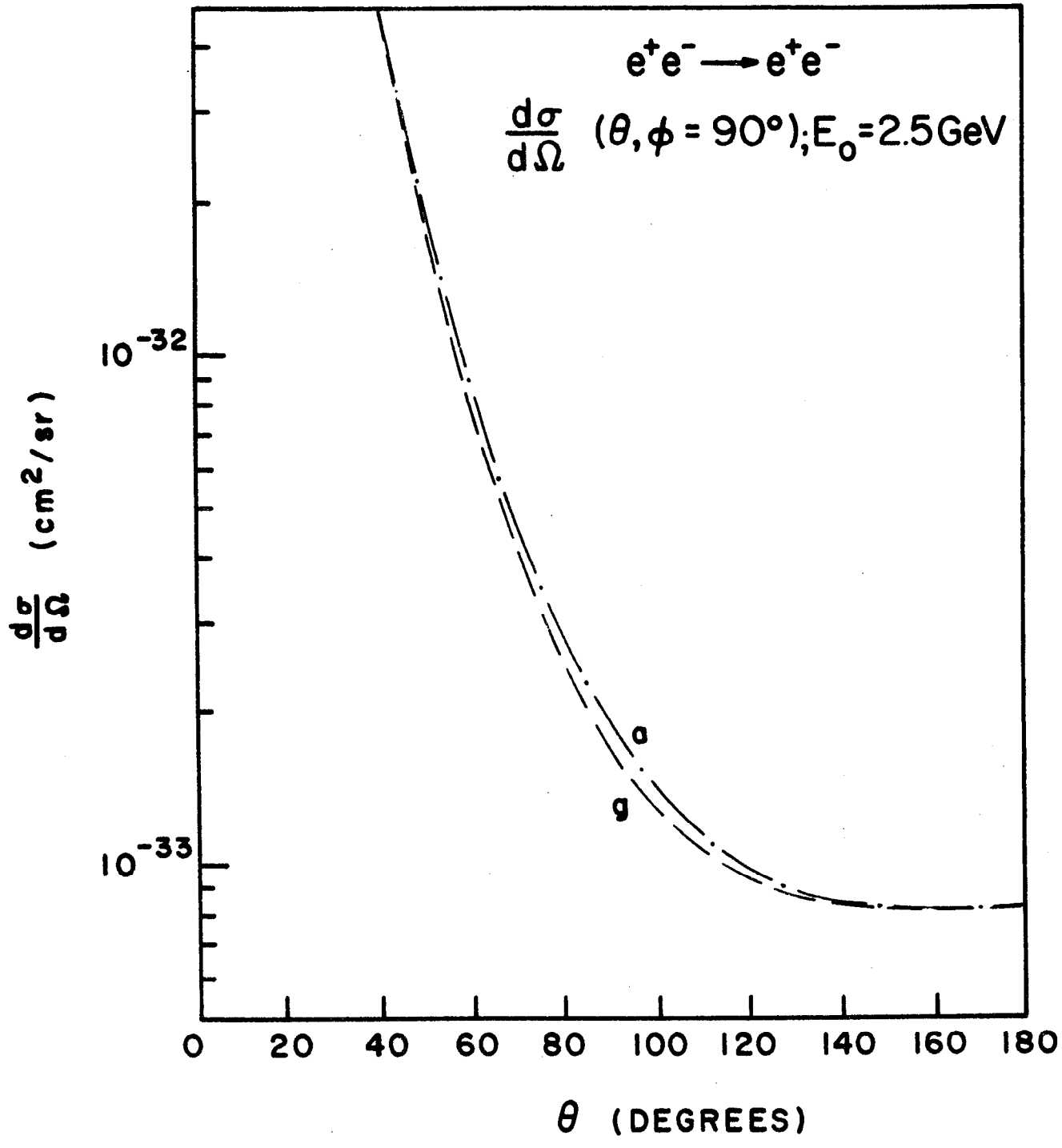
$e^+e^- \longrightarrow e^+e^-$
$\frac{d\sigma}{d\Omega}$ $(\theta, \phi = 90°); E_0 = 2.5\,GeV$
10^{-32}
10^{-33}
$\frac{d\sigma}{d\Omega}$ (cm^2/sr)
a
g
0
20
40
60
80
100
120
140
160
180
θ (DEGREES)

Fig. 11

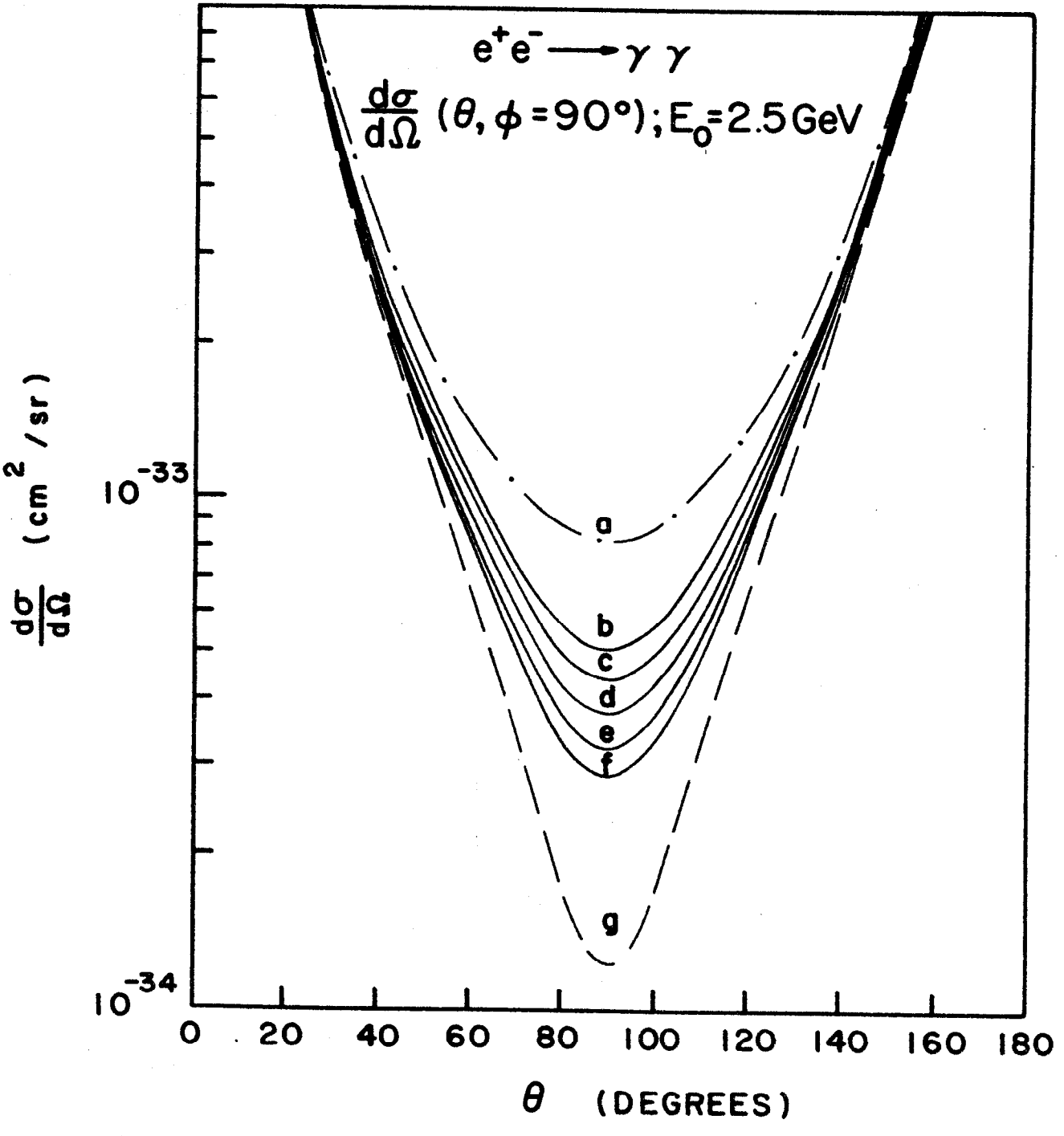
$e^+e^- \longrightarrow \gamma\gamma$
$\frac{d\sigma}{d\Omega}(\theta, \phi = 90°); E_0 = 2.5\,GeV$
$\frac{d\sigma}{d\Omega}$ (cm^2/sr)
10^{-33}
10^{-34}
a
b
c
d
e
f
g
0 20 40 60 80 100 120 140 160 180
θ (DEGREES)

Fig. 12

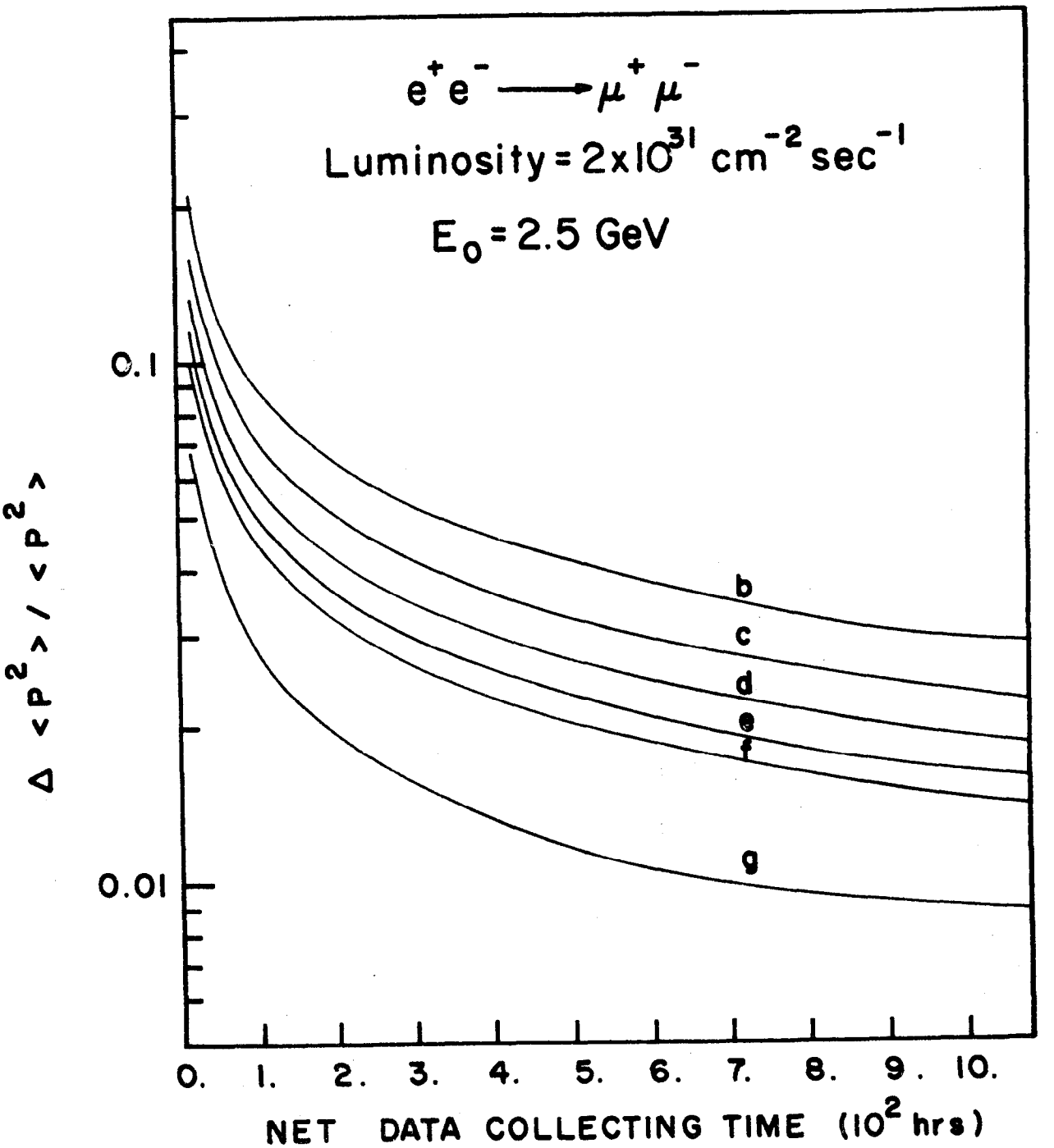
$e^+e^- \longrightarrow \mu^+\mu^-$
Luminosity = 2×10^{31} cm^{-2} sec^{-1}
E_0 = 2.5 GeV
0.1
0.01
$\Delta \langle P^2 \rangle / \langle P^2 \rangle$
b
c
d
e
f
g
0. 1. 2. 3. 4. 5. 6. 7. 8. 9. 10.
NET DATA COLLECTING TIME (10^2 hrs)

Fig. 13

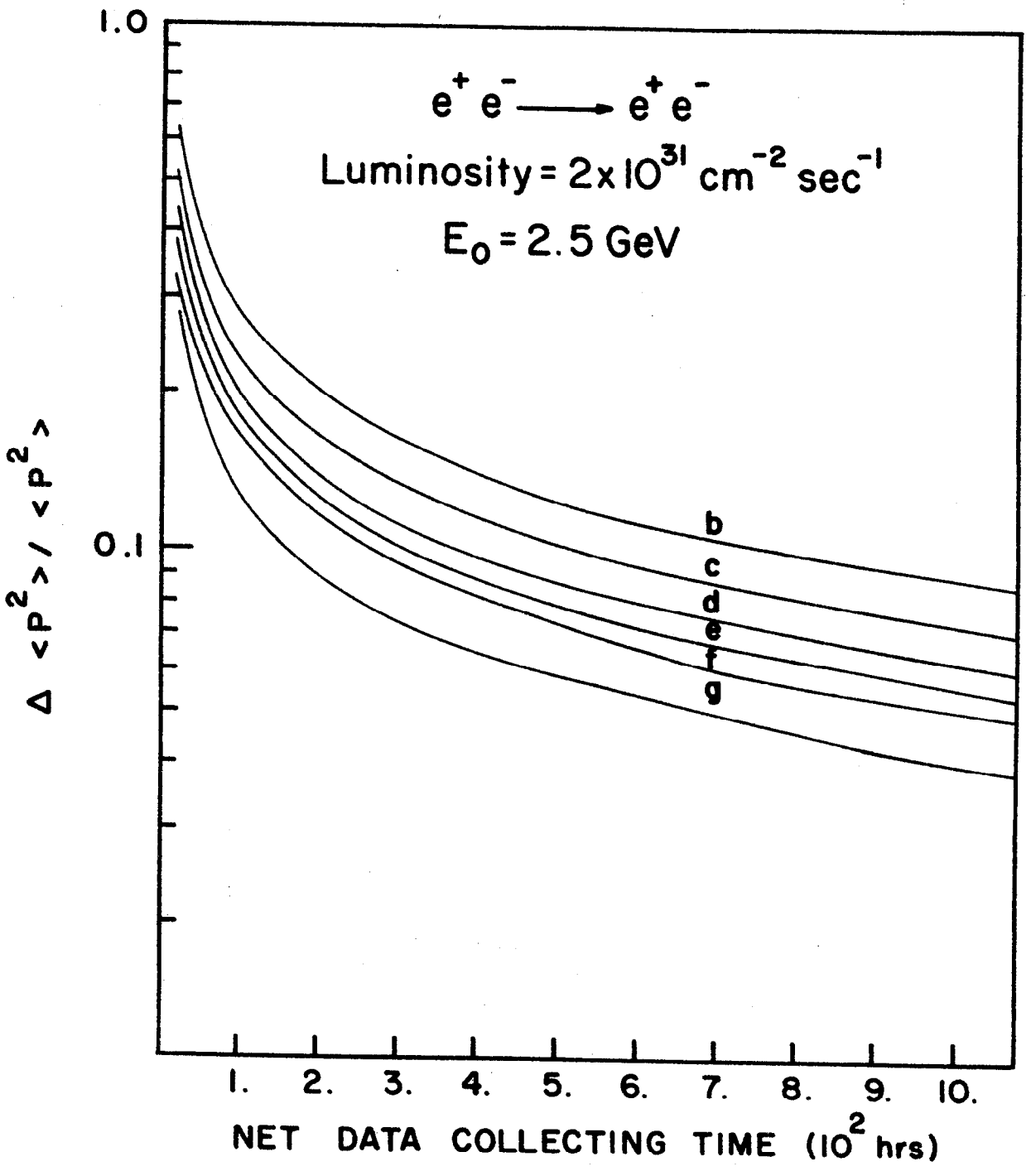
1.0
0.1
$e^+ e^- \longrightarrow e^+ e^-$
Luminosity = 2×10^{31} cm^{-2} sec^{-1}
$E_0 = 2.5$ GeV
b
c
d
e
f
g
$\Delta \langle P^2 \rangle / \langle P^2 \rangle$
1. 2. 3. 4. 5. 6. 7. 8. 9. 10.
NET DATA COLLECTING TIME (10^2 hrs)

Fig. 14

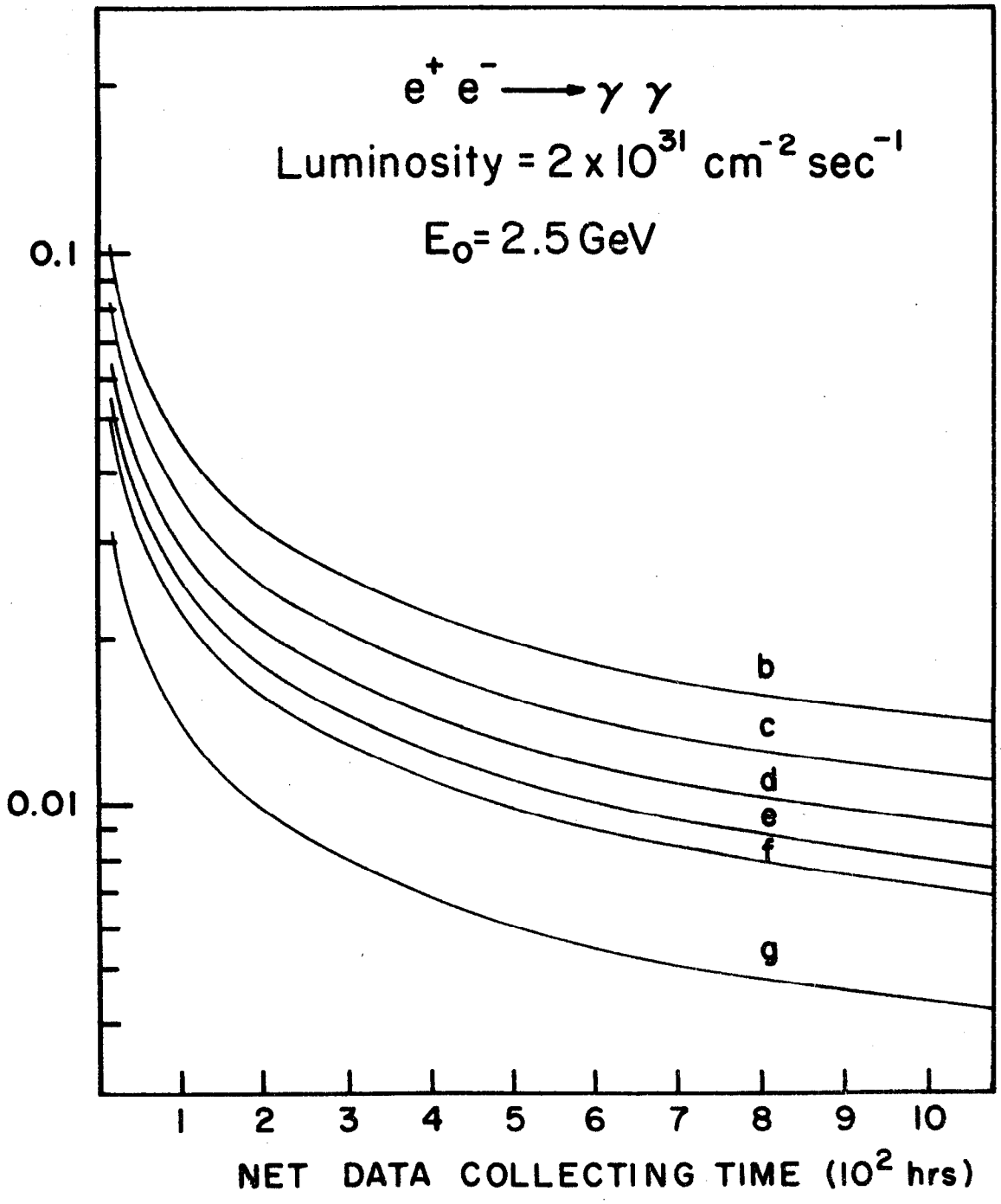
$e^+ e^- \longrightarrow \gamma\ \gamma$
Luminosity = 2×10^{31} cm^{-2} sec^{-1}
E_0= 2.5 GeV
0.1
0.01
b
c
d
e
f
g
1
2
3
4
5
6
7
8
9
10
NET DATA COLLECTING TIME (10^2 hrs)

Fig. 15

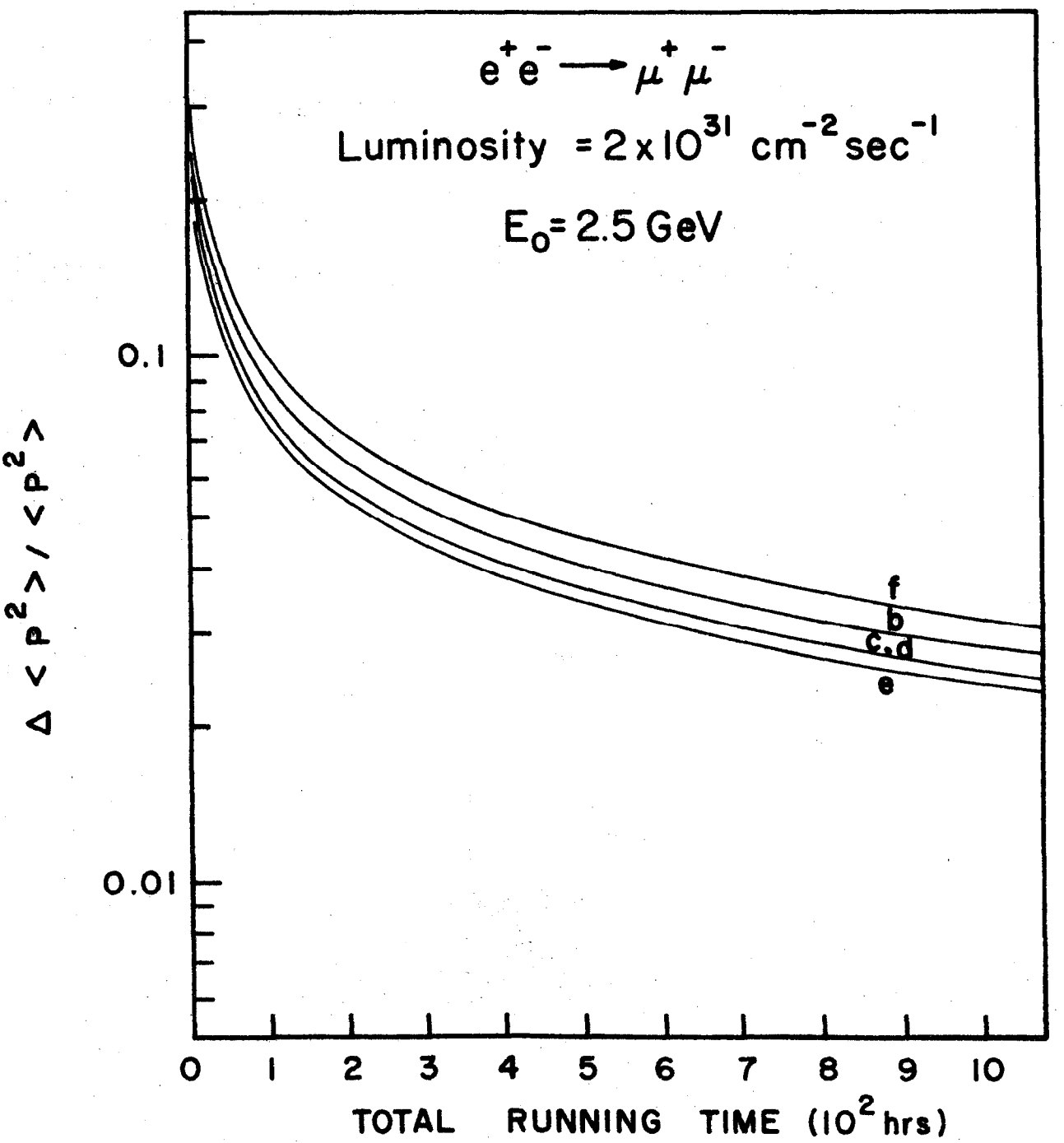
$e^+e^- \longrightarrow \mu^+\mu^-$
Luminosity $= 2 \times 10^{31}$ cm^{-2}sec^{-1}
$E_0 = 2.5$ GeV
0.1
0.01
$\Delta < p^2 > / < p^2 >$
f
b
c,d
e
0 1 2 3 4 5 6 7 8 9 10
TOTAL RUNNING TIME (10^2 hrs)

Fig. 16